

INFLIGHT ESTIMATION OF MAGNETOMETER BIASES
 FOR THE ACTIVE MAGNETOSPHERIC PARTICLE
 TRACER EXPLORERS (AMPTE) MISSION

(NASA-CP-1992) INFLIGHT ESTIMATION OF
 MAGNETOMETER BIASES FOR THE ACTIVE
 MAGNETOSPHERIC PARTICLE TRACER EXPLORERS
 (AMPTE) MISSION (Computer Sciences Corp.)

19/18 Unclassified
 0109624 N92-70850

Prepared for
 GODDARD SPACE FLIGHT CENTER
 By
 COMPUTER SCIENCES CORPORATION

Under
 Contract NAS 5-24300
 Task Assignment 41506

Prepared by:

G. F. Neal 28 May 81
 Dr. G. F. Neal Date

G. F. Neal 28 May 81
 For Dr. R. H. Thompson Date

Approved by:

W. V. Myers 5/28/81
 W. V. Myers Date
 Section Manager

D. R. Sood 5/28/81
 Dr. D. R. Sood Date
 Department Manager

ABSTRACT

This document presents an analysis and the simulated test results of two algorithms, RESIDT and RESIDG, which were developed to estimate the residual biases for an orthogonal triad of magnetometers. The algorithms were tested under the simulated flight conditions of the Active Magnetospheric Particle Tracer Explorers (AMPTE) mission for sensitivity to data rate, sensor granularity, orbit position, magnitude of residual bias, and sensor misalignment. On the basis of these test results, conclusions were drawn concerning the type of data necessary to ensure good algorithm performance.

TABLE OF CONTENTS

<u>Section 1 - Introduction</u>	1-1
1.1 Overview	1-1
1.2 AMPTE Mission	1-2
<u>Section 2 - Equations for Magnetometer Bias Determination</u>	2-1
<u>Section 3 - RESIDG Algorithm</u>	3-1
3.1 General Description	3-1
3.2 Existing Software	3-2
<u>Section 4 - RESIDT Algorithm</u>	4-1
4.1 General Description of the Iterative Solution	4-1
4.1.1 Convergence Properties	4-2
4.1.2 Specific Example of Convergence	4-4
4.1.3 Equations for Bias Uncertainties	4-6
4.2 Software Description	4-10
<u>Section 5 - AMPTE Engineering Simulator Runs</u>	5-1
5.1 Spacecraft Ephemeris	5-1
5.2 Geomagnetic Field Simulation Results	5-1
5.3 Earth Occultation Simulation Results	5-4
<u>Section 6 - Test Procedures and Results</u>	6-1
6.1 Software Driver Development	6-1
6.2 Test Objectives	6-1
6.3 Magnetometer Bias Magnitude Test Results -	
Ideal Data	6-1
6.4 Data Period and Sensor Granularity Test Results	6-5
6.5 Nonproximity to Perigee Test Results	6-18
6.6 Sensor Misalignment Test Results	6-22
<u>Section 7 - Conclusions</u>	7-1
7.1 Sensitivity to Data Period	7-1
7.2 Sensitivity to Sensor Granularity	7-1
7.3 Sensitivity to Magnetometer Biases	7-2
7.4 Sensitivity to Perigee Proximity	7-2
7.5 Sensitivity to Sensor Misalignment	7-3
7.6 Recommended Bias Determination Algorithm	7-3
7.7 Necessity for Simultaneous Data Readings	7-3
<u>References</u>	

LIST OF ILLUSTRATIONS

Figure

3-1	RESIDG Software Calling Hierarchy.	3-4
4-1	RESIDT Bias Solutions as a Function of Numerical Iterations	4-8
4-2	RESIDT System Baseline Diagram	4-11
5-1	Sample AMPTE Engineering Simulator Output. .	5-2
5-2	Magnitude of the Major Component of the Geomagnetic Field	5-5
6-1	Simulated Accuracy of RESIDG for Granularity Value of 1.6 mG.	6-13
6-2	Simulated Accuracy of RESIDG for Granularity Value of 3.2 mG.	6-14
6-3	Simulated Accuracy of RESIDG for Granularity Value of 5.0 mG.	6-15
6-4	Simulated Accuracy of RESIDG for Granularity Value of 8.0 mG.	6-16
6-5	Simulated Accuracy of RESIDG for Granularity Value of 14.0 mG	6-17
6-6	RESIDG and RESIDT Results for the 1.6 mG Resolution (Bias Vector = 5, 10, 15 mG) . . .	6-19
6-7	RESIDG and RESIDT Results for the 1.6 mG Resolution (Bias Vector = 40, 60, 80 mG) . .	6-20
6-8	Accuracy Versus Sensor Granularity	6-21
6-9	Computed Accuracy Versus Start Time for RESIDG and RESIDT	6-25
6-10	Computed Accuracy Versus X-Axis Misalignment	6-28

LIST OF TABLES

4-1	Bias Determination Calculation for $B/H << 1$. . .	4-5
4-2	Bias Determination Calculation for $B >> H$	4-7
4-3	Core Requirements for RESIDT and RESIDG Modules	4-12
6-1	Tests of Magnetometer Bias Magnitude Using RESIDG - Ideal Data.	6-3
6-2	Tests of Magnetometer Bias Magnitude Using RESIDT - Ideal Data.	6-4
6-3	RESIDG Data Period and Sensor Granularity Test Results	6-6
6-4	RESIDT Data Period and Sensor Granularity Test Results	6-9
6-5	RESIDG Orbit Dependence Results.	6-23
6-6	RESIDT Orbit Dependence Results.	6-24
6-7	Effects of Magnetometer Misalignment	6-27

SECTION 1 - INTRODUCTION

1.1 OVERVIEW

Experience in attitude determination using magnetic field measurements has shown that the inflight calibration of magnetometers is essential to meeting attitude accuracy requirements in the error range of 2 to 3 degrees (Reference 1). This document presents the results of the tests of two algorithms, RESIDT and RESIDG, which were developed to estimate the residual biases for an orthogonal triad of magnetometers under the simulated flight conditions of the Active Magnetospheric Particle Tracer Explorers (AMPTE) mission.

The RESIDT algorithm was developed by Computer Sciences Corporation (CSC) specifically for this study. The technical details of its formulation are discussed in detail in this report. The RESIDG algorithm was developed for a previous mission; the computer code was extracted from that of the Solar Maximum Mission (SMM). RESIDG is the only piece of previously existing software that is attitude-independent and suitable for AMPTE, and which has a code that is adaptable and thoroughly modularized.

Section 2 presents a general formulation of the inflight residual bias determination problem. Sections 3 and 4 discuss the RESIDT and RESIDG algorithms in relation to the general formulation. Section 5 discusses the orbital conditions and attitude constraints assumed for this study and the results of the AMPTE Engineering Simulator (Reference 2) runs. In addition, some observations based on that data are presented. Section 6 presents the tests made to simulate the effects of items such as data period, sensor granularity, and sensor misalignment, and includes the test results. Section 7 presents the conclusions that are evident from the results of this study.

1.2 AMPTE MISSION

The AMPTE mission is a small Explorer-class international cooperative program between the Bundesministerium fuer Forschung und Technologie (BMFT) of the Federal Republic of Germany (FRG) and the National Aeronautics and Space Administration (NASA). Two spacecraft, the Charge Composition Explorer (CCE), which is provided by NASA, and the Ion Release Module (IRM), which is provided by the FRG, will investigate the detailed physical processes operating within the magnetosphere-ionosphere domain using active experimentation (Reference 3). The concept involves the release, by the IRM, of tracer ions outside the magnetosphere and within the solar wind at the subsolar point as well as at various other points, including the magnetospheric tail, while the highly eccentric IRM orbit precesses. The CCE instrumentation will detect released ions inside the magnetosphere and will perform other charge-detection experiments independent of ion releases (Reference 3).

Only the attitude determination subsystem and planned orbital conditions of the CCE are addressed in this document. The CCE will be injected into a highly eccentric orbit with perigee altitude of 300 kilometers and apogee attitude of 7.5 Earth radii (Reference 3). The spacecraft attitude will be spin stabilized, and the CCE will carry a digital Sun sensor and a three-axis orthogonal magnetometer triad. The spin axis will lie in the orbital plane, and the angle between the spin axis and the Sun line will be minimized.

SECTION 2 - EQUATIONS FOR MAGNETOMETER BIAS DETERMINATION

Development of a formalism that is independent of spacecraft attitude requires a loss function that is independent of spacecraft attitude. A loss function that satisfies this criterion is described in this section.

The quantities used throughout this section are defined as follows:

$H_j^{(i)}$ = jth component of the model magnetic field in the geocentric inertial (GCI) system at position i

$M_j^{(i)}$ = jth magnetometer reading at position i

B_j = jth magnetometer bias which is taken to be independent of the spacecraft position

For the ith point, an error $\delta^{(i)}$ is defined by the following equation:

$$\delta^{(i)} = \vec{H}^{(i)}^2 - \vec{M}^{(i)}^2 - \vec{B}^2 + 2\vec{M}^{(i)} \cdot \vec{B} \quad (2-1)$$

The objective of this equation is to minimize quantity $\delta^{(i)}$ by adjusting the bias vector B to its optimal value. Thus, the loss function to be minimized is given by

$$L(\vec{B}) = \sum_{i=1}^N \omega^{(i)} \delta^{(i)}^2 \quad (2-2)$$

where $\omega^{(i)}$ = the weight associated with the ith data point.

The weights are assumed to be normalized to unity, that is

$$\sum_{i=1}^N \omega^{(i)} = 1 \quad (2-3)$$

Determining the minimum value of $L(\vec{B})$ first requires that its derivatives with respect to the components of the bias vector be set equal to zero:

$$\frac{\partial L}{\partial B_\alpha} = 0 \quad (2-4)$$

where

$$\frac{\partial L}{\partial B_\alpha} = -4 \sum_{i=1}^N \omega^{(i)} \left[\vec{H}^{(i)}^2 - \left(\vec{B} - \vec{M}^{(i)} \right)^2 \right] \left(B_\alpha - M_\alpha^{(i)} \right) \quad (2-5)$$

Combining Equations (2-3), (2-4), and (2-5) leads to the following result:

$$\sum_{k=1}^3 O_{\alpha k} B_k = b_\alpha + F_\alpha(\vec{B}) \quad (2-6)$$

where

$$O_{\alpha k} = \delta_{\alpha k} (\langle H^2 \rangle - \langle M^2 \rangle) - 2 \langle M_\alpha M_k \rangle$$

$$b_\alpha = \langle M_\alpha H^2 \rangle - \langle M_\alpha M \rangle^2$$

$$F_\alpha(\vec{B}) = (\vec{B}_\alpha - \langle M_\alpha \rangle) \vec{B}^2 - 2 B_\alpha \vec{B} \cdot \langle \vec{M} \rangle$$

$$\langle A \rangle = \sum_{i=1}^N \omega^{(i)} A^{(i)}$$

$$\delta_{\alpha k} = 1 \text{ if } k = \alpha; = 0 \text{ if } k \neq \alpha$$

Equation (2-6) can be solved directly to obtain the best value for the bias vector \vec{B} .

SECTION 3 - RESIDG ALGORITHM

3.1 GENERAL DESCRIPTION

RESIDG is an attitude-independent method for determining residual magnetometer biases for an orthogonal magnetometer triad flown onboard a spacecraft. Reference 4 contains a detailed mathematical description of RESIDG.

RESIDG minimizes the loss function given in Equation (2-2). In Equation (2-1), only the magnetic field components are treated as independent parameters. The resulting problem, a least-squares fit to a quadratic equation, is solved by using an iterative procedure which converges to the exact solution if the biases are much smaller than the magnetometer readings themselves.

RESIDG approaches the solution to the problem in two steps. First, RESIDG obtains a trial solution for the biases. Then, RESIDG iterates a linearized form of Equation (2-6) until a precise solution is obtained.

The trial solution is determined by minimizing the following loss function:

$$L'(\vec{B}) = L(\vec{B}) - \langle \delta(\vec{B}) \rangle^2 \quad (3-1)$$

where

$$\langle \delta(\vec{B}) \rangle = \sum_{i=1}^N \omega^{(i)} \delta^{(i)}(\vec{B})$$

$\delta^{(i)}(\vec{B})$ is given by Equation (2-1) and $L(\vec{B})$ is the loss function given by Equation (2-2). The equations for \vec{B} , which result when $L(\vec{B})$ is minimized, are linear in \vec{B} and, therefore, are simpler to solve. When the magnetometer data

is ideal (i.e., no noise or measurement error exists), $\langle \delta(\vec{B}_T) \rangle = 0$, where \vec{B}_T is the true bias. In this case, $L'(\vec{B}_T) = L(\vec{B}_T) = 0$ and the same value of \vec{B} minimizes both $L'(\vec{B})$ and $L(\vec{B})$. The solution to the linear problem, therefore, is precisely the same as the solution to the non-linear problem, and the trial solution is exact.

A problem arises with this process when noise and inexact measurements are present in the data. In those cases, the loss functions $L'(\vec{B})$ and $L(\vec{B})$ will, in general, be minimized by quite different values of \vec{B} . The trial solution will be completely different from the true solution. This is illustrated theoretically in Reference 4 and experimentally with real spacecraft data (Reference 1). Thus, in general, it should be expected that the RESIDG trial solution will be quite different from the actual least-squares solution with real data.

After the trial solution is obtained, RESIDG then linearizes Equation (2-6) and uses a Newton-Raphson scheme with the trial function described previously as a first guess to obtain a solution. Convergence is defined as the point at which the input and output values agree to within a present tolerance.

3.2 EXISTING SOFTWARE

The RESIDG algorithms are implemented in a set of several FORTRAN subroutines, which are invoked by a call to the main subroutine RESIDG. For this study, the RESIDG software was obtained from the ground-support software for the SMM, for which it was used for inflight determination of biases for the SMM magnetometers (Reference 3). To facilitate interfacing, the SMM routine MAGBAS also was retained, because all the arrays and parameters were set up essentially as they were needed for this study. However, task personnel

did develop a driver routine to provide the necessary program functions for exercising the existing software (Section 6.1).

Figure 3-1 is a block diagram of the RESIDG routines as implemented in this study. Reference 3 describes the calling sequences and other features of the RESIDG software.

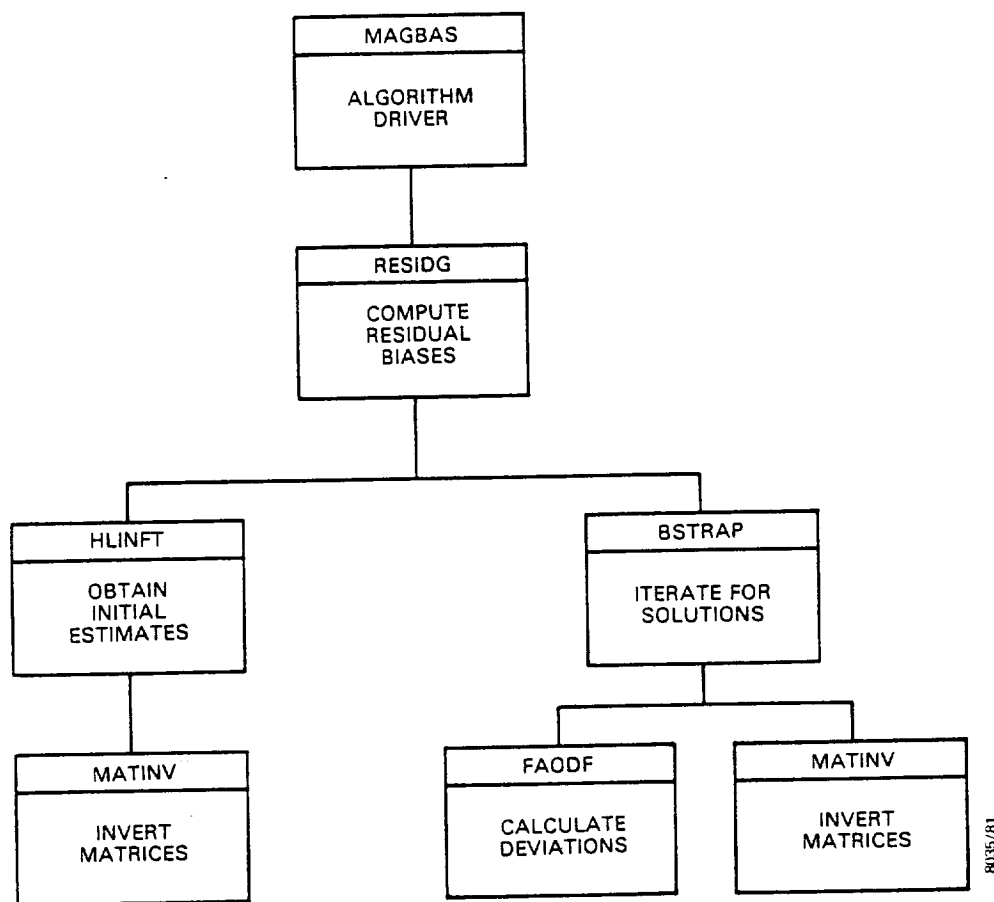


Figure 3-1. RESIDG Software Calling Hierarchy

SECTION 4 - RESIDT ALGORITHM

4.1 GENERAL DESCRIPTION OF THE ITERATIVE SOLUTION

Equation (2-6) is nonlinear in terms of the bias vector. In general, an analytic solution to this type of equation is not available; however, the construction of a numerical solution is possible.

The method chosen during this study to the solution to Equation (2-6) is an iterative procedure. The zero-th order, or trial solution to Equation (2-6), is obtained by dropping the nonlinear terms in comparison to the linear terms. This approximation is valid only when the bias is small in comparison with the actual magnetic field. This point is not critical, as the iteration scheme constructs an accurate solution even when the trial solution is not close to the true solution. The trial solution is given by

$$B_k^{(0)} = \sum_{\alpha=1}^3 (O^{-1})_{k\alpha} b_\alpha \quad (4-1)$$

where O^{-1} = inverse of the matrix O

$B_k^{(0)}$ = trial solution

This solution may be iterated as follows:

$$B_k^{(1)} = B_k^{(0)} + \sum_{\delta=1}^3 (O^{-1})_{k\delta} F_\delta (\vec{B}^{(0)})$$
$$\vdots \quad (4-2)$$

$$B_k^{(j)} = B_k^{(0)} + \sum_{\delta=1}^3 (O^{-1})_{k\delta} F_\delta (\vec{B}^{(j-1)})$$

The iteration continues until

$$\text{ABS} \left(\frac{B_k^{(j)} - B_k^{(j-1)}}{B_k^{(j)}} \right) < \epsilon \quad (4-3)$$

where ϵ = some arbitrarily small value depending on the accuracy desired.

4.1.1 CONVERGENCE PROPERTIES

The investigation of the convergence properties of the iterative solution given by Equation (4-2) requires the analysis of a related problem. Consider a scalar field $H^{(i)}$ which is determined from a field model at position i . The corresponding measured field is $M^{(i)}$, and the bias to be determined is denoted by B . The analogous loss function to that given by Equation (2-2) is

$$L(B) = \sum_{i=1}^N \omega^{(i)} \delta^{(i)}^2 \quad (4-4)$$

where

$$\delta^{(i)} = H^{(i)}^2 - M^{(i)}^2 - B^2 + 2M^{(i)}B \quad (4-5)$$

The resulting equation, whose solution minimizes the loss function of Equation (4-4), is given by

$$OB = b + F(B) \quad (4-6)$$

where

$$O = \langle H^2 \rangle - 3 \langle M^2 \rangle$$

$$b = \langle H^2 M \rangle - \langle M^3 \rangle$$

$$F(B) = B^3 - 3B^2 \langle M \rangle$$

The nth iterative solution to Equation (4-6) is written as

$$B^{(n)} = B_{\text{TRUE}} + \epsilon_n \quad (4-7)$$

where B_{TRUE} = the exact solution to Equation (4-6)

ϵ_n = the error of the iterative solution after
n iterations

Combining Equations (4-6) and (4-7) leads to the following
result:

$$0\epsilon_{n+1} = \frac{\partial F}{\partial B} \epsilon_n \quad (4-8)$$

where

$$\frac{\partial F}{\partial B} = 3B(B - 2\langle M \rangle) \quad (4-9)$$

Thus, the ratio of successive errors is

$$\frac{\epsilon_{n+1}}{\epsilon_n} \approx \frac{3B(B - 2\langle M \rangle)}{\langle H^2 \rangle - 3\langle M^2 \rangle} \quad (4-10)$$

Two limits to Equation (4-10) should be considered. First,
in the case, $B/H \ll 1$, Equation (4-10) reduces to

$$\frac{\epsilon_{n+1}}{\epsilon_n} \approx \frac{3B\langle H \rangle}{\langle H^2 \rangle} \quad (4-11)$$

Equation (4-11) indicates rapid convergence of the iterative solution, because $\epsilon_{n+1}/\epsilon_n$ is of the order B/H which has been assumed to be small.

For $B \gg H$, then, Equation (4-10) reduces to

$$\frac{\epsilon_{n+1}}{\epsilon_n} = 1 \quad (4-12)$$

For this case, the solution would converge very slowly.

Equation (4-10) yields only qualitative results for the real three-dimensional magnetometer bias determination problem; however, it is expected that the general conclusions will be valid as illustrated by Equations (4-11) and (4-12).

4.1.2 SPECIFIC EXAMPLE OF CONVERGENCE

The AMPTE engineering data simulator (Reference 2) was used to generate biased magnetometer data to investigate the convergence properties of RESIDT. Two cases were considered in approximating the limiting values discussed in Section 4.1.1-- $B/H \ll 1$ and $B/H \gg 1$.

The first case considered was $B/H \ll 1$; in this case, 200 data points were included in the calculation. Data that included the perigee point at which the magnetic field attains its maximum value was used. The magnetic field can be resolved into a component along the AMPTE spin axis, $H_{||}$, and a component perpendicular to the spin axis, H_{\perp} .

The maximum or perigee values for these components are $H_{\perp}^{MAX} = 240$ milligauss (mG) and $H_{||}^{MAX} = 90$ mG. The input biases are 5 mG, 10 mG, and 15 mG along the x, y, and z spin axes, respectively. The results of the bias determination calculation using RESTDT are shown in Table 4-1.

Rapid convergence and very high accuracy is obtained. The trial solution $B^{(0)}$, which corresponds to iteration 0 in

Table 4-1. Bias Determination Calculation for $B/H \ll 1$

ITERATION NUMBER	LOSS FUNCTION	B_x (mG)	B_y (mG)	B_z (mG)
0	54621.0	5.00288	12.0278	15.0213
1	5153.0	4.98344	9.38109	14.9473
2	370.0	5.00481	10.1647	15.0152
3	29.0	4.99870	9.95352	14.9959
4	2.0	5.00037	10.0128	15.0012
5	0.2	4.99990	9.99635	14.9997
6	0.01	5.00003	10.0009	15.0001

8035/81

NOTES:

NUMBER OF DATA POINTS = 200

$H_{\perp}^{MAX} = 240$ mG

$H_{\parallel}^{MAX} = 90$ mG

TRUE BIASES:

B_x (mG) = 5

B_y (mG) = 10

B_z (mG) = 15

Table 4-1, initially was not accurate in the y component and needed to be iterated to obtain satisfactory results.

Investigation of the case in which $B \gg H$ uses a subset of the data used in the first test. Here, 100 data points well outside the perigee region are used. For this test, $H_1^{\text{MAX}} = 5 \text{ mG}$ and $H_{||}^{\text{MAX}} = 2 \text{ mG}$. As before, the input biases are 5 mG, 10 mG, and 15 mG. These results are presented in Table 4-2 and Figure 4-1. In this case, convergence is very slow and incomplete, as predicted in Section 4.1.1.

4.1.3 EQUATIONS FOR BIAS UNCERTAINTIES

The square of the magnitude of the computed magnetic field at point i is given by

$$g^{(i)} = M^{(i)}^2 + B^2 - 2\vec{M}^{(i)} \cdot \vec{B} \quad (4-13)$$

The error covariance matrix P_{ik}^g is

$$P_{ik}^g = \frac{\partial B_k}{\partial g^{(i)}} \quad (4-14)$$

The relation between the computed magnetic field uncertainty $\delta g^{(i)}$ and the uncertainty in the bias δB_k is

$$\delta B_k = \sum_{i=1}^N P_{ik}^g \delta g^{(i)} \quad (4-15)$$

Using Equation (4-13), the covariance matrix may be evaluated as follows:

$$P_{ik}^g = \frac{1}{2(B_k - M_k^{(i)})} \quad (4-16)$$

Table 4-2. Bias Determination Calculation for $B \gg H$

ITERATION NUMBER	LOSS FUNCTION	B_x (mG)	B_y (mG)	B_z (mG)
0	24100.0	1.8	2.8	5.3
10	1460.0	3.7	5.5	11.0
20	501.0	4.1	6.1	12.4
30	240.0	4.4	6.3	13.1
40	133.0	4.5	6.5	13.6
50	81.0	4.6	6.6	13.9

8035/81

NOTES:

NUMBER OF DATA POINTS = 100

$H_{\perp}^{\text{MAX}} = 5$ mG

$H_{\parallel}^{\text{MAX}} = 2$ mG

TRUE BIASES:

B_x (mG) = 5

B_y (mG) = 10

B_z (mG) = 15

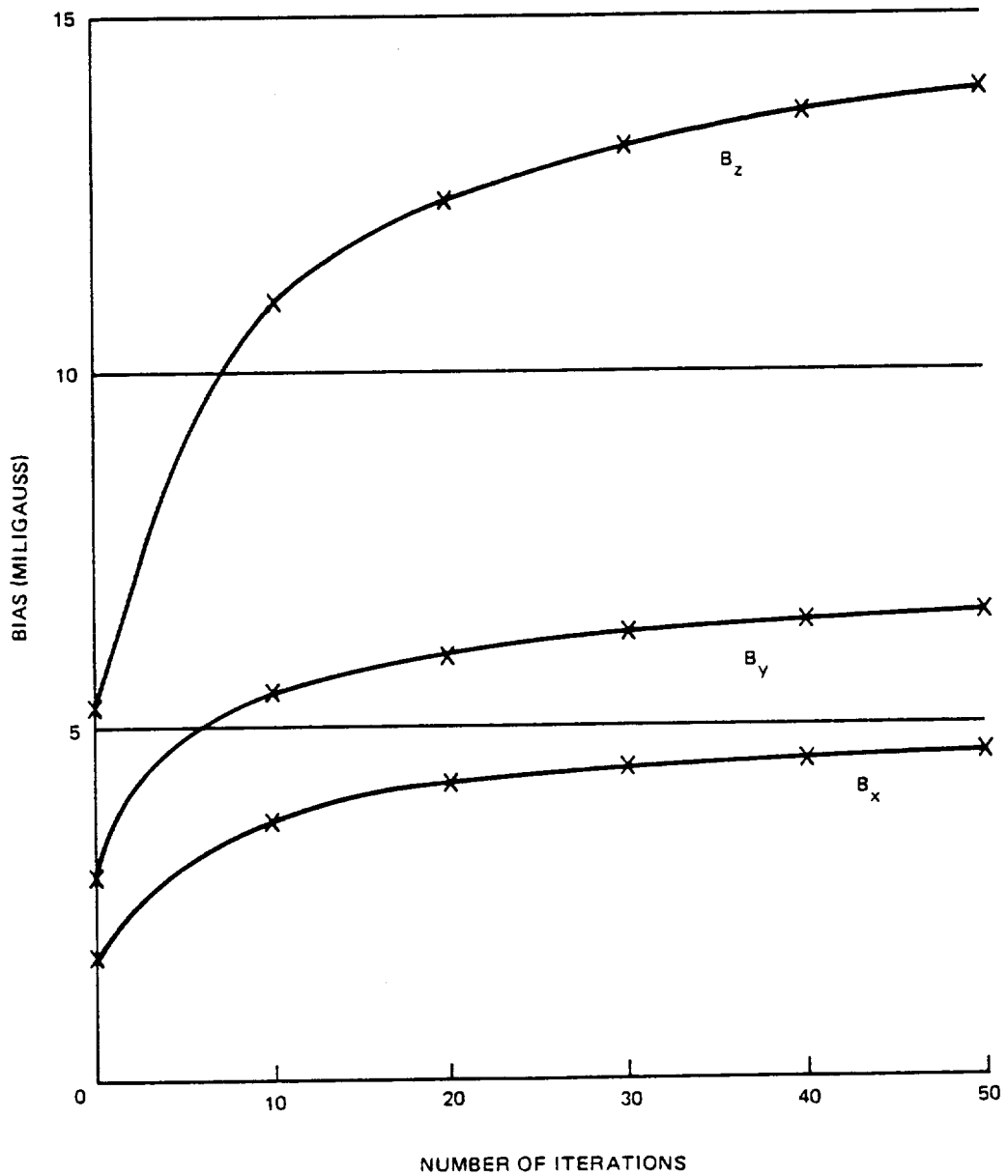


Figure 4-1. RESIDT Bias Solutions as a Function of Numerical Iterations

The quantity $\delta g^{(i)}$ is related to the uncertainty in the magnetometer reading $\delta M_\lambda^{(i)}$ by

$$\delta g^{(i)} = \sum_{\lambda=1}^3 P_{i\lambda}^M \delta M_\lambda^{(i)} \quad (4-17)$$

where

$$P_{i\lambda}^M = \frac{\partial g^{(i)}}{\partial M_\lambda^{(i)}} = -2 \left(B_\lambda - M_\lambda^{(i)} \right) \quad (4-18)$$

The mean square uncertainties are related by

$$\delta g^{(i)2} = \sum_{\lambda=1}^3 \left(P_{i\lambda}^M \right)^2 \delta M_\lambda^{(i)2} \quad (4-19)$$

It is assumed that $\delta M_\lambda^{(i)} = \delta M_\lambda$ (i.e., the uncertainty in the magnetometer reading) is independent of component and position. Therefore, the following result is obtained:

$$\delta g^{(i)2} = 4g^{(i)} \delta M^2 \quad (4-20)$$

Using Equations (4-14), (4-16), and (4-20), the final result is given by

$$\delta B_k = \delta M \left(\sum_{i=1}^N \frac{g^{(i)}}{\left(B_k - M_k^{(i)} \right)^2} \right)^{1/2} \quad (4-21)$$

Equation (4-21) shows that if the bias components are comparable to the measurement, large uncertainties in the resulting biases will result.

4.2 SOFTWARE DESCRIPTION

Like RESIDG, the RESIDT algorithm is a collection of FORTRAN-callable subroutines (Figure 4-2). RESIDT is invoked by a call to subroutine RESIDT, with the other routines generally being transparent to the user. The following table describes the call argument parameters. These parameters appear in the table in the order in which they would be placed in an actual call to the routine.

Name	Type	I/O	Description
FLDSQD(1)	R*8	I	Magnitude of the model magnetic field squared (mG^2)
FLDMES(I,J)	R*8	I	The Jth component of the measured field (mG) at position I. The I index is dimensioned to NDIM and the J index is dimensioned to three
NDIM	I*4	I	Row dimension of FLDMES (NDIM,3)
NGOOD	I*4	I	Number of actual data points
ANOISE	R*8	I	Magnetometer noise level (mG)
EPS	R*8	I	Convergence parameter for iterative solution determined by BIASCL
ITERMX	I*4	I	Maximum number of iterations in BIASCL
IDEBUG	I*4	I	If IDEBUG = 0, no debug printout is written
IOUT	I*4	I	FORTRAN unit number for debug output
BIAS(3)	R*8	O	Computed biases (mG)
WEIGHT(1)	R*8	O	Computer normalized weights
IERR	I*4	O	Return code for BIASCL

Table 4-3 shows the core requirements in an IBM S/360-95 computer for both RESIDG and RESIDT.

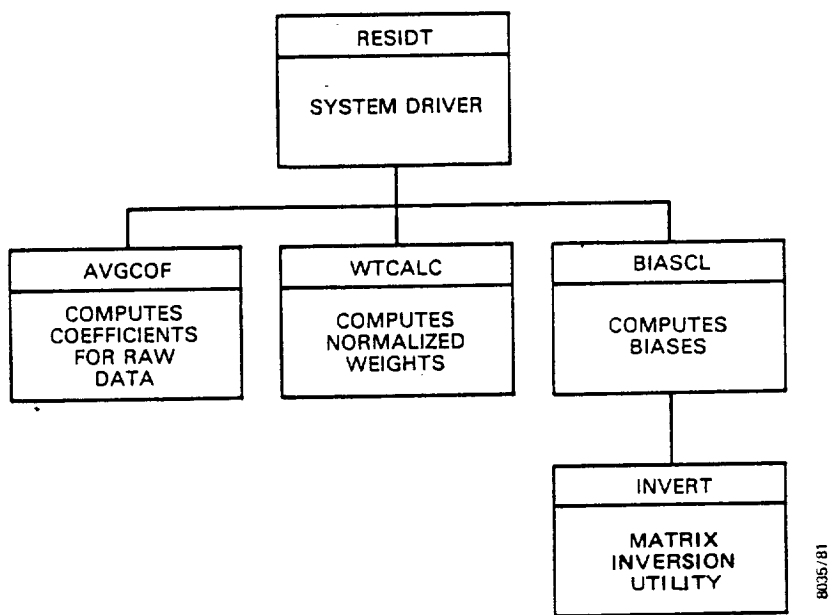


Figure 4-2. RESIDT System Baseline Diagram

Table 4-3. Core Requirements for RESIDT and RESIDG Modules

RESIDT MODULE		RESIDG MODULE	
SUBROUTINE	CORE REQUIREMENT (BYTES)*	SUBROUTINE	CORE REQUIREMENT (BYTES)*
RESIDT	0.92K	RESIDG	7.0K
WT CALC	0.63K	HLINFT	3.7K
AVGCOF	2.3K	BSTRAP	3.6K
BIASCL	1.9K	FAODF	0.36K
INVERT	1.7K 7.5K (TOTAL)	MATINV	1.5K 16.2K (TOTAL)

*DATA ARRAYS ARE DIMENSIONED FOR 200 POINTS

SECTION 5 - AMPTE ENGINEERING SIMULATOR RUNS

This section describes the orbital conditions and attitude constraints assumed for the purpose of this study and the general results of the AMPTE simulator runs.

5.1 SPACECRAFT EPHEMERIS

The Keplerian orbital elements needed in this study are as follows (Reference 2):

- Semimajor axis--30446.2 kilometers
- Eccentricity--0.780657
- Inclination--0.0 degrees
- Argument of perigee--90.0 degrees
- Right ascension of the ascending node--90.0 degrees
- Mean anomaly--320.0 degrees
- Epoch (YYMMDD.HHMMSS)--830901.000000

In this configuration, the major axis of the elliptical orbit lies approximately along the projection of the Earth/Sun line on the orbit planes with apogee toward the Sun.

5.2 GEOMAGNETIC FIELD SIMULATION RESULTS

Figure 5-1 contains two pages of a sample printout from an AMPTE engineering simulator run which used the orbital elements defined in Section 5.1. In the sample run, data is generated every 15 seconds from a time well before perigee (which occurs at approximately 830901.013800)¹ to a time 22 minutes after perigee. The quantities shown are

- Spacecraft GCI position vector in kilometers
- Model geomagnetic field vector in the GCI (mG)
- Angle between the spin axis and the Sun line (degrees)

¹Time in format YYMMDD.HHMMSS.

AMPT-E FREQUENCY SPECTRUM CUTOUT TRACER RECORD

RIGHT ASCENSION OF SPIN AXIS IN GCI (DEGS). ----- 159.67227173

DECINATION OF SPIN AXIS IN GCI (DEGS). ----- 0.00000010

SATELLITE SPIN RATE (DEGS/SEC). ----- 55.55555993

ANGULAR DISPLACEMENT OF ECEF FRAME FROM TRUE SPIN FRAME AT TIME=0 (DEGS). ----- 0.0

DIRECTION COSINES OF CCAFE SLN SENSER AXES IN THE BODY FRAME. ----- 0.0
0.0
0.0

DIRECTION COSINES OF MAGNETOMETER X-AXIS WITH RESPECT TO ROTATING FRAME. ----- 1.00000000
0.0
0.0

DIRECTION COSINES OF MAGNETOMETER Y-AXIS WITH RESPECT TO ROTATING FRAME. ----- 0.0
1.00000000
0.0

DIRECTION COSINES OF MAGNETOMETER Z-AXIS WITH RESPECT TO ROTATING FRAME. ----- 0.0
0.0
1.00000000

SPIN AXIS COORDINATE IN NOMINAL SPIN FRAME. ----- 89.55555985

SPIN AXIS AZIMUTH IN NOMINAL SPIN FRAME. ----- 65.55555985

BIAS ALONG MAGNETOMETER X-AXIS (MG). ----- 0.0

BIAS ALONG MAGNETOMETER Y-AXIS (MG). ----- 0.0

BIAS ALONG MAGNETOMETER Z-AXIS (MG). ----- 0.0

MAGNETOMETER INSTRUMENTAL SENSITIVITY (MG) ----- 0.00000000

SIN SENSOF INSTRUMENTAL RESOLUTION (DEG) ----- 0.0

SIN SENSOF BIAS (DEG) ----- 0.0

Figure 5-1. Sample AMPTE Engineering Simulator Output (1 of 2)

Figure 5-1 Sample AMPT Engineering Simulator Output (2 of 2)

- Earth to Sun unit vector in the GCI
- Components of the magnetic field in the spacecraft fixed coordinate system (Reference 2)

A spin rate of 10 revolutions per minute (rpm) was assumed (Reference 3).

Figure 5-2 presents a plot of the major component of the geomagnetic field (the component that is perpendicular to the equatorial plane) against the time in minutes from perigee. The data was derived from the sample run in Figure 5-1. The magnitude of this component falls to about 50 mG (about 20 percent of perigee value) after 25 minutes from perigee. The simulator run illustrated in Figure 5-1 showed that the distribution is symmetric about perigee. The computed maximum value of the major component of the geomagnetic field at perigee is about 240 mG. The total magnitude (rms) at perigee is about 265 mG.

Work from previous missions, in particular the Solar Maximum Mission (SMM), indicates that the magnetic field should be in excess of approximately 50 mG for the magnetometers to be effective in determining spacecraft attitude. In addition, the data sample should include several variations in the strength of the field (Reference 1). In accordance with these findings, the simulator results indicate that the magnetometers may be effective only within about a 50-minute window around perigee (perigee \pm 25 minutes). The effects of proximity to perigee on algorithm performance are discussed in Section 6.

5.3 EARTH OCCULTATION SIMULATION RESULTS

Given the zero-degree inclination of the CCE orbit and the relatively low altitude at perigee, the periods during which the CCE Sun sensor will be occulted by the Earth are of particular interest. The occultation algorithm in the AMPTE

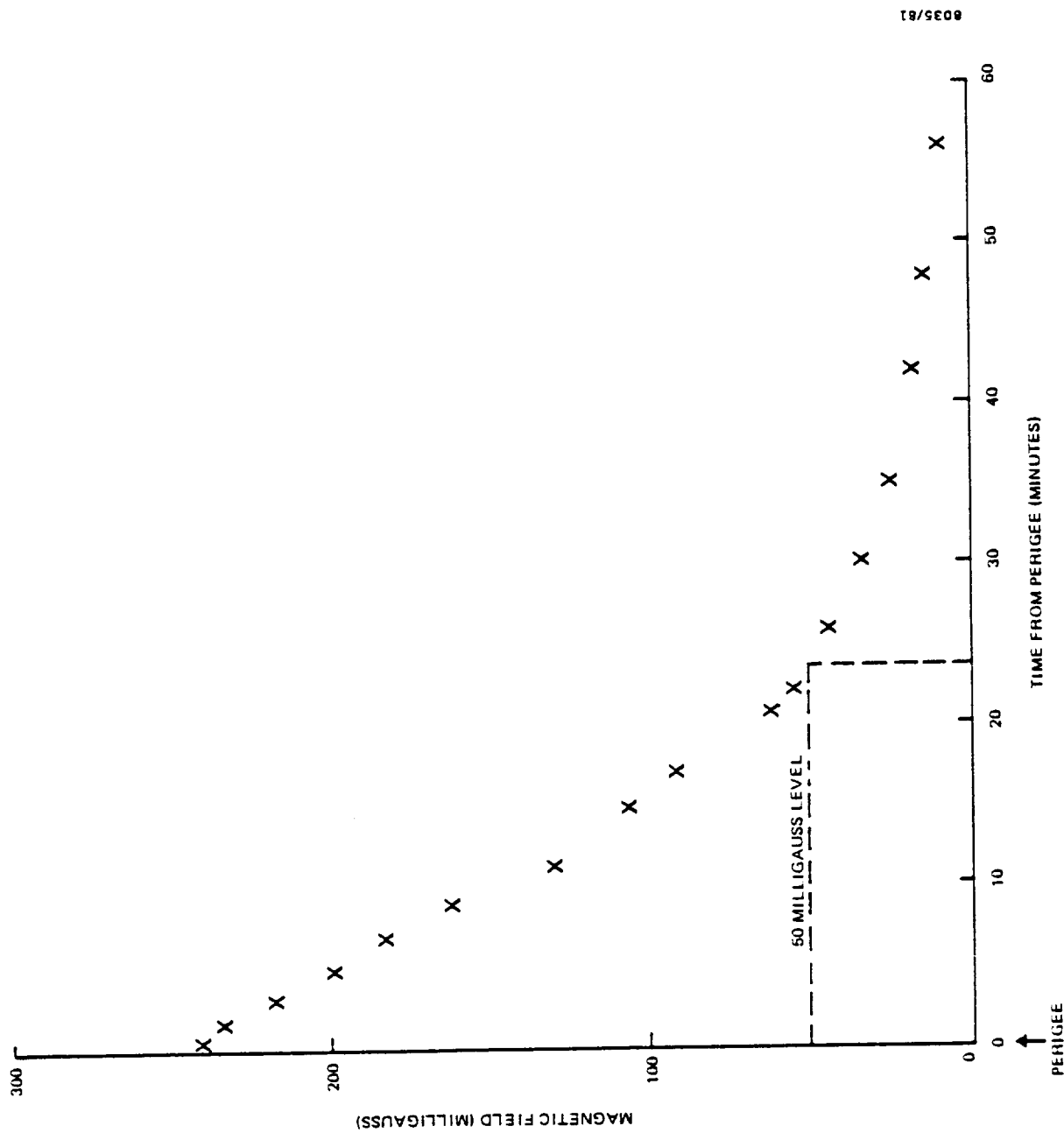


Figure 5-2. Magnitude of the Major Component of the Geomagnetic Field

engineering simulator is that of a simple cylindrical model (Reference 2). Basically, the angle between the spacecraft-to-Earth vector and a spacecraft-to-perpendicular-Earth radius vector is used as a reference. The sensor is considered occulted whenever the angle between the spacecraft-to-Earth vector and spacecraft-to-Sun vector falls below this reference. A sample result of this computation is shown in Figure 5-1; YES and NO in the right-most column indicate that the Sun is or is not occulted, respectively.

The AMPTE simulator runs indicate that the sensor will be occulted from roughly 13 minutes before perigee until 4 minutes after perigee, given that the apogee-perigee line is Sun pointing. Thus, Sun data will not be available for roughly one-third of the time during which optimal magnetometer data is available. As long as the CCE attitude remains constant, however, this may not be a problem. An essentially unlimited amount of Sun data will be available away from perigee.

SECTION 6 - TEST PROCEDURES AND RESULTS

The RESIDG and RESIDT magnetometer bias algorithms were tested to determine the variation of simulated results as a function of changes in the simulated engineering characteristics of the sensors. This section describes the tests that were run and the test results.

6.1 SOFTWARE DRIVER DEVELOPMENT

Because both RESIDG and RESIDT are in the form of FORTRAN subroutines, a driver module was developed to exercise the software. The driver routine provides for NAMELIST input that allows pertinent parameters to be varied. It also provides for the printing of results and important intermediate quantities. The subroutine that reads the AMPTE Interface Data Set (AIDS) was also included in the software package (Reference 2).

6.2 TEST OBJECTIVES

For this study, two major objectives were defined:

- First objective--To determine the performance (i.e., accuracy) of the magnetometer bias determination algorithms under varying conditions of magnetometer bias magnitude, data period, sensor granularity, orbital position (proximity to perigee), and sensor misalignment.
- Second objective--Given the test data determined by the above studies, to present specific engineering conclusions that would guide AMPTE Project engineers in selecting AMPTE hardware and software components.

6.3 MAGNETOMETER BIAS MAGNITUDE TEST RESULTS - IDEAL DATA

Several tests were made using "ideal" data to determine the effects of increasing bias magnitude on the RESIDT and

RESIDG algorithms. Ideal data is that which does not include the effects of sensor granularity. (For comparison, the tests described in the following subsections do include sensor granularity). Tables 6-1 and 6-2 show the test cases run and the test results for the tests using ideal data. Note that the biases simulated ranged from x, y, z components of 5, 10, and 15 mG up to 60, 80, and 100 mG, and that the data periods simulated were 10, 20, 30, and 60 seconds.

In the tests shown in Tables 6-1 and 6-2, the RESIDG algorithm was given the same initial bias estimate as that computed by RESIDT. The RESIDG algorithm has the capability of taking this initial estimate from NAMELIST input, whereas RESIDT cannot. These procedures were followed, however, to ensure equal testing conditions for both algorithms.

The results of the tests in Tables 6-1 and 6-2, and in succeeding tables are reported in terms of "accuracy" with accuracy defined as

$$M = \left[\sum_{i=1}^3 (B_i - B'_i)^2 \right]^{1/2} \quad (6-1)$$

where the B_i values are the simulated biases for the x, y, and z axes, and the B'_i values are the calculated biases.

Table 6-1 shows that the overall accuracy of the RESIDG algorithm was very good--2 mG or less for the cases in which the solution did converge. As expected, the accuracy decreased slightly with increased magnetometer bias and decreased data frequency.

At and above the biases of 40, 60, and 80 mG (which represent about 35 percent of the maximum geomagnetic field at perigee), RESIDG begins to break down. Two of the solutions diverged.

Table 6-1. Tests of Magnetometer Bias Magnitude Using RESIDG - Ideal Data

SIMULATED BIASES (MILLIGAUSS)			DATA PERIOD (SECONDS)			ITERATIONS TO CONVERGE			RESIDG RESULTS (MILLIGAUSS)						
X	Y	Z	X	Y	Z	X	Y	Z	X	Y	Z	X	Y	Z	ACCURACY
COMPONENT	COMPONENT	COMPONENT	DEVIATION	DEVIATION	DEVIATION	COMPONENT	DEVIATION	COMPONENT	DEVIATION	COMPONENT	DEVIATION	DEVIATION	DEVIATION	DEVIATION	
5	10	15	10	7	6.0	0.0	10.0	0.0	16.0	0.0	0.0	0.0	0.0	0.0	0.0
6	10	15	20	10	5.0	0.0	10.0	0.0	15.0	0.0	0.0	0.0	0.0	0.0	0.0
5	10	15	30	14	5.0	0.0	10.0	0.0	15.0	0.0	0.0	0.0	0.0	0.0	0.0
5	10	15	60	16	5.0	0.0	10.0	0.0	15.0	0.0	0.0	0.0	0.0	0.0	0.0
20	30	40	10	6	20.1	-0.1	30.5	-0.5	40.1	-0.1	-0.1	0.52	-0.1	0.1	0.1
20	30	40	20	13	20.0	0.0	30.0	0.0	40.1	0.1	-0.1	0.1	-0.1	0.1	0.1
20	30	40	30	18	19.6	0.4	30.0	0.0	39.9	0.1	0.1	0.41	0.1	0.41	0.41
20	30	40	60	20	19.6	0.4	30.0	0.0	39.9	0.1	0.1	0.41	0.1	0.41	0.41
20	40	60	10	9	20.0	0.0	40.0	0.0	60.0	0.0	0.0	0.0	0.0	0.0	0.0
20	40	60	20	14	20.0	0.0	40.0	0.0	60.0	0.0	0.0	0.0	0.0	0.0	0.0
20	40	60	30	20	19.5	0.5	39.9	0.1	59.8	0.2	0.2	0.54	0.1	0.54	0.54
20	40	60	60	22	19.5	0.5	39.9	0.1	59.8	0.2	0.2	0.54	0.0	0.54	0.54
40	60	80	10	11	40.0	0.0	60.0	0.0	80.0	0.0	0.0	0.0	0.0	0.0	0.0
40	60	80	20	15	40.0	0.0	60.0	0.0	80.1	-0.1	-0.1	0.1	-0.1	0.1	0.1
40	60	80	30	21	38.3	1.7	59.4	0.6	79.4	0.6	0.6	1.90	0.5	1.93	1.93
40	60	80	60	23	38.2	1.8	59.5	0.5	79.5	0.5	-	-	-	-	-
60	80	40	10	*	*	*	*	*	*	*	*	*	*	*	*
80	40	60	10	11	80.0	0.0	40.0	0.0	60.0	0.0	0.0	0.0	0.0	0.0	0.0
60	80	100	10	*	*	*	*	*	*	*	*	*	*	*	*

DIVERGED

Table 6-2. Tests of Magnetometer Bias Magnitude Using RESIDT - Ideal Data

SIMULATED BIASES (MILLIGAUSS)			DATA PERIOD (SECONDS)		ITERATIONS TO CONVERGE		RESIDT RESULTS (MILLIGAUSS)									
X	Y	Z	X	Y	Z	X	COMPONENT	X DEVIATION	Y	COMPONENT	Z	COMPONENT	X DEVIATION	Y DEVIATION	Z DEVIATION	ACCURACY
5	10	15	10	7	5.0	0.0	10.0	0.0	15.0	0.0	0.0	0.0	0.0	0.0	0.0	0.0
5	10	15	20	4	5.0	0.0	10.0	0.0	15.0	0.0	0.0	0.0	0.0	0.0	0.0	0.0
5	10	16	30	19	4.98	0.02	9.99	0.01	15.0	0.0	0.0	0.0	0.0	0.0	0.0	0.02
5	10	16	60	19	5.0	0.0	10.0	0.0	15.0	0.0	0.0	0.0	0.0	0.0	0.0	0.0
20	30	40	10	5	20.0	0.0	30.0	0.0	40.0	0.0	0.0	0.0	0.0	0.0	0.0	0.0
20	30	40	20	10	20.0	0.0	30.0	0.0	40.0	0.0	0.0	0.0	0.0	0.0	0.0	0.0
20	30	40	30	43	19.9	0.1	29.8	0.2	40.0	0.0	0.0	0.0	0.0	0.0	0.0	0.22
20	30	40	60	46	19.8	0.2	29.8	0.2	40.0	0.0	0.0	0.0	0.0	0.0	0.0	0.28
20	40	60	10	7	20.0	0.0	40.0	0.0	60.0	0.0	0.0	0.0	0.0	0.0	0.0	0.0
20	40	60	20	17	20.0	0.0	39.9	0.1	60.0	0.0	0.0	0.0	0.0	0.0	0.0	0.1
20	40	60	30	58	19.7	0.3	39.6	0.4	60.0	0.0	0.0	0.0	0.0	0.0	0.0	0.50
20	40	60	60	61	19.6	0.4	39.6	0.4	59.9	0.1	80.0	0.0	0.0	0.0	0.1	0.57
40	60	80	10	15	40.0	0.0	59.9	0.1	80.0	0.0	0.0	0.0	0.0	0.0	0.0	0.1
40	60	80	20	29	40.0	0.0	59.7	0.3	79.9	0.1	99.9	0.1	0.1	0.1	0.1	0.32
40	60	80	30	74	38.9	0.1	58.8	1.2	79.8	0.2	99.8	0.2	0.2	0.2	0.2	1.22
40	60	80	60	78	38.8	0.2	58.6	1.4	79.8	0.2	99.8	0.2	0.2	0.2	0.2	1.43
60	80	40	10	17	60.0	0.0	79.9	0.1	40.0	0.0	0.0	0.0	0.0	0.0	0.0	0.1
80	40	60	10	14	80.0	0.0	40.0	0.0	60.0	0.0	0.0	0.0	0.0	0.0	0.0	0.0
60	80	100	10	16	60.0	0.0	79.8	0.2	100.0	0.0	0.0	0.0	0.0	0.0	0.0	0.2

Table 6-2 shows that the overall accuracy of the RESIDT algorithm, like the RESIDG algorithm, is very good under ideal conditions. The overall errors ranged from zero to about 1-1/2 mG. As was the case in Table 6-1, the RESIDT algorithm shows that accuracy decreased slightly with increasing magnetometer bias magnitude and decreasing data frequency. However, one significant attribute of the RESIDT algorithm was that it did converge for all the test cases, whereas the RESIDG algorithm diverged for two of the test cases.

More extensively detailed and realistic (granularity included) tests are described in Section 6.4.

6.4 DATA PERIOD AND SENSOR GRANULARITY TEST RESULTS

Tests for the combined effects of data frequency and sensor granularity were conducted for both the RESIDG and RESIDT algorithms. For RESIDG, the tests used the initial bias estimates from the RESIDG initial estimator. As stated previously, RESIDT generates its own initial estimate of the biases.

Tables 6-3 and 6-4 show the tests that were run using the RESIDG and RESIDT algorithms, respectively. The left-hand columns show that magnetometer biases of x, y, z component values of 5, 10, 15 and 40, 60, 80 mG were simulated. For each combination of magnetometer bias, sensor granularities of 1.6 mG, 3.2 mG, 5.0 mG, 8.0 mG, and 14.0 mG were simulated. With each combination of bias magnitude and sensor granularity, solutions were obtained for data periods ranging from 6 seconds to 42 seconds in increments of 2 seconds.

The right-hand columns in Tables 6-3 and 6-4 show the computed magnetometer bias for each (x, y, z) component, and the deviation of the computed bias from the simulated bias.

Table 6-3. RESIDG Data Period and Sensor Granularity Test Results (1 of 3)

Table 6-3. RESIDG Data Period and Sensor Granularity Test Results (2 of 3)

Table 6-3. RESIDG Data Period and Sensor Granularity Test Results (3 of 3).

Table 6-4. RESIDT Data Period and Sensor Granularity Test Results (1 of 3)

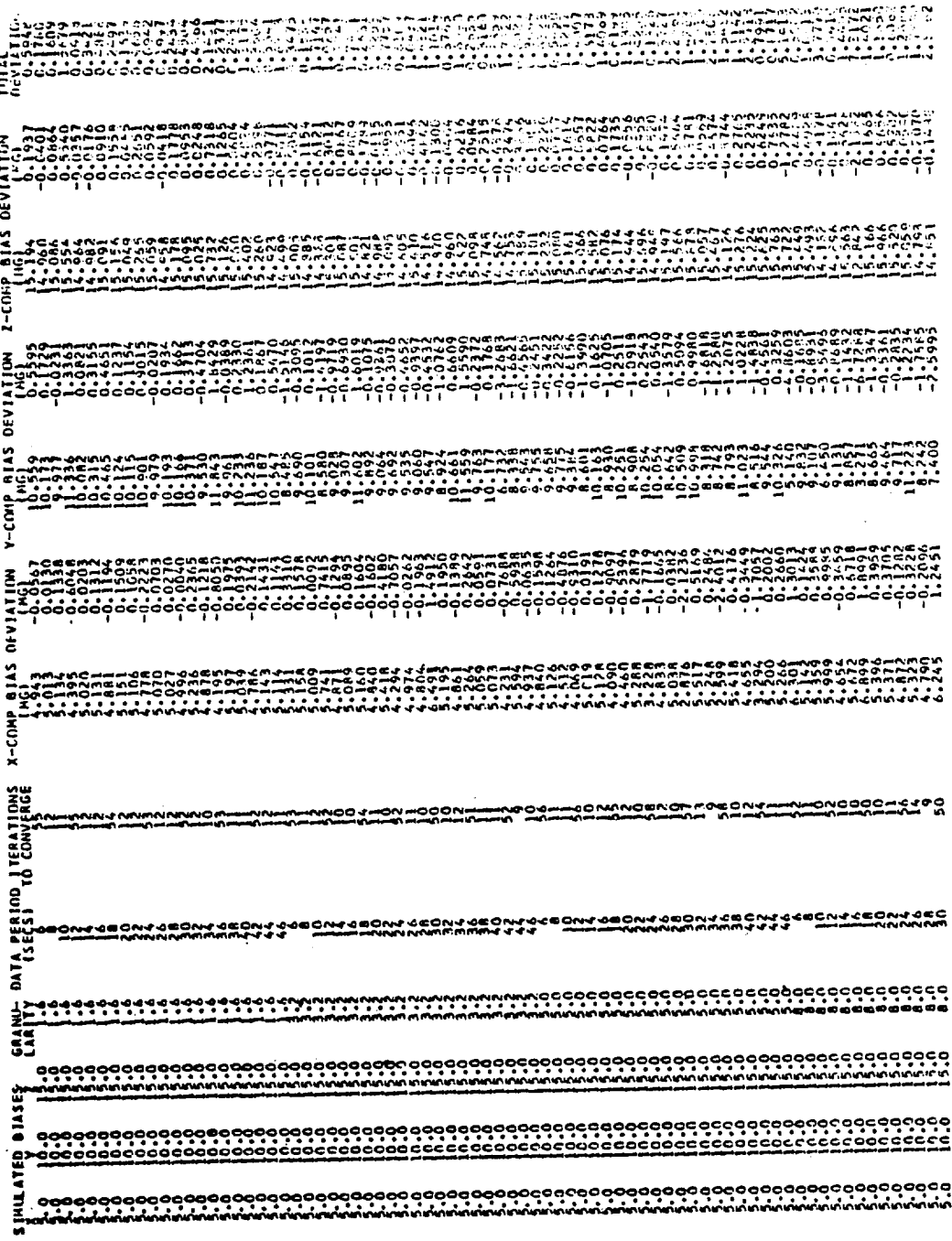


Table 6-4. RESIDT Data Period and Sensor Granularity Test Results (2 of 3)

Table 6-4. RESIDT Data Period and Sensor Granularity Test Results (3 of 3)

GRANULARITY	DATA PERIOD (SECS)	ITERATIONS TO CONVERGE
1	1	1
2	1	1
4	1	1
8	1	1
16	1	1
32	1	1
64	1	1
128	1	1
256	1	1
512	1	1
1024	1	1
2048	1	1
4096	1	1
8192	1	1
16384	1	1
32768	1	1
65536	1	1
131072	1	1
262144	1	1
524288	1	1
1048576	1	1
2097152	1	1
4194304	1	1
8388608	1	1
16777216	1	1
33554432	1	1
67108864	1	1
134217728	1	1
268435456	1	1
536870912	1	1
1073741824	1	1
2147483648	1	1
4294967296	1	1
8589934592	1	1
17179869184	1	1
34359738368	1	1
68719476736	1	1
137438953472	1	1
274877906944	1	1
549755813888	1	1
1099511627776	1	1
2199023255552	1	1
4398046511104	1	1
8796093022208	1	1
17592186044416	1	1
35184372088832	1	1
70368744177664	1	1
140737488355328	1	1
281474976710656	1	1
562949953421312	1	1
1125899906842624	1	1
2251799813685248	1	1
4503599627370496	1	1
9007199254740992	1	1
18014398509481984	1	1
36028797018963968	1	1
72057594037927936	1	1
14411518807585968	1	1
28823037615171936	1	1
57646075230343872	1	1
115292150460687744	1	1
230584300921375488	1	1
461168601842750976	1	1
922337203685501952	1	1
184467407137100384	1	1
368934814274200768	1	1
737869628548401536	1	1
147573925709680312	1	1
295147851419360624	1	1
590295702838721248	1	1
118059140567744256	1	1
236118281135488512	1	1
472236562270977024	1	1
944473124541954048	1	1
1888946249083908096	1	1
3777892498167816192	1	1
7555784996335632384	1	1
15111569992671264768	1	1
30223139985342529536	1	1
60446279970685059072	1	1
12089255994137011816	1	1
24178511988274023632	1	1
48357023976548047264	1	1
96714047953096094528	1	1
19342809590619218956	1	1
38685619181238437912	1	1
77371238362476875824	1	1
154742476724953751648	1	1
309484953449857503296	1	1
618969906899715006592	1	1
1237939813799430013184	1	1
2475879627598860026368	1	1
4951759255197720052736	1	1
9903518510395440010472	1	1
19807036206908800020944	1	1
39614072413817600041888	1	1
79228144827635200083776	1	1
158456289655270400167552	1	1
31691257931054080033504	1	1
63382515862108160067008	1	1
12676503172421632013416	1	1
25353006344843264026832	1	1
50706012689686528053664	1	1
10141202537937305610732	1	1
20282405075874611221464	1	1
40564810151749222442928	1	1
81129620303498444885856	1	1
16225924060699688971760	1	1
32451848121399377943520	1	1
64903696242798755887040	1	1
129807392485597511774080	1	1
259614784971195023548160	1	1
519229569942387547096320	1	1
1038459139884775094192640	1	1
2076918279769550188385280	1	1
4153836559539100376770560	1	1
8307673119078200753541120	1	1
1661534623815600150708240	1	1
3323069247631200301416480	1	1
6646138495262400602832960	1	1
13292276990528001205665920	1	1
26584553981056002411331840	1	1
53169107962112004822663680	1	1
106338215924224009645327360	1	1
212676431848448019290654720	1	1
425352863696896038581309440	1	1
850705727393792077162618880	1	1
1701411454787584154325237760	1	1
3402822909575168308650475520	1	1
6805645819150336617300851040	1	1
13611291638300673234601602080	1	1
27222583276601346469203204160	1	1
54445166553202692938406408320	1	1
108890332106405385876812816640	1	1
217780664212810771753625633280	1	1
435561328425621543507251266560	1	1
871122656851243087014502533120	1	1
1742245313702486174029050066240	1	1
3484490627404972348058100132480	1	1
6968981254809944696116200264960	1	1
13937962509619889392232400529840	1	1
27875925019239778784464801059680	1	1
55751850038479557568929602119360	1	1
11150370076855911513789204238720	1	1
22300740153711823027578408477440	1	1
44601480307423646055156816954880	1	1
89202960614847292110313633909760	1	1
178405921229694584220673667819520	1	1
356811842459389168441347335639040	1	1
713623684918778336882694671278080	1	1
1427247369837566673765389342556160	1	1
2854494739675133347530778685112320	1	1
5708989479350266695061557370224640	1	1
1141797895870053339012314674044920	1	1
2283595791740106678024629348089840	1	1
4567191583480213356049258696179680	1	1
9134383166960426712098517392359360	1	1
18268766333920853424196346784718720	1	1
36537532667841706848392693569437440	1	1
73075065335683413696785387138874880	1	1
14615013071366827339357077427774960	1	1
29230026142733654678714154855549840	1	1
58460052285467309357428309711099680	1	1
11692010450933461871456619422199360	1	1
23384020801866923742913238844398720	1	1
46768041603733847485826477688795440	1	1
93536083207467694971652955377590880	1	1
18707216641493538994330511075518160	1	1
37414433282987077988661022151036320	1	1
74828866565974155977322044302072640	1	1
149657733131948311954644088604145280	1	1
299315466263896623909288177208290560	1	1
598630932527793247818576354416581120	1	1
1197261865055864956237532708833162240	1	1
2394523730111729912475065417666324480	1	1
4789047460223459824950130835332648960	1	1
9578094920446919649800261670665297920	1	1
19156189840893839299600523341330595840	1	1
38312379681787678599201046682661191680	1	1
76624759363575357198402093365322383360	1	1
153249518727150714396804187310644767200	1	1
306498537454301428793608374621289534400	1	1
612997074908602857587216749242578568800	1	1
1225994149817205715174433498485157137600	1	1
2451988299634411430348866996970315355200	1	1
4903976599268822860697733993940630710400	1	1
9807953198537645721395467987881261420800	1	1
19615906397075291442789935975762528401600	1	1
39231812794150582885579871951525556803200	1	1
78463625588301165771159743903051113606400	1	1
15692725117660231154231948780610223212800	1	1
31385450235320462308463897561220446425600	1	1
62770900470640924616927795122440893252800	1	1
125541800941281849233855902244817866505600	1	1
251083601882563698467711804489635733011200	1	1
502167203765127396935423608979271466022400	1	1
1004334407325254793870867217958542932044800	1	1
2008668814650509587741734435917085864089600	1	1
4017337629301019175483468871834171728179200	1	1
8034675258602038350966937743668343456358400	1	1
1606935051720407670193875547333666691316800	1	1
3213870103440815340387751094667333382633600	1	1
6427740206881630680775522189334666765267200	1	1
1285548041376326136155104437866933353134400	1	1
2571096082752652272302208875733866706288000	1	1
51421921655053045446044177514677334031760000	1	1
102843843310106090892088355029354668063520000	1	1
205687686620212181784176710058709336130400000	1	1
411375373240424363568353420117418672268800000	1	1
822750746480848727136706840234837344537600000	1	1
164550149296169745427341368046775488915200000	1	1
329100298592339490854682736093550977824000000	1	1
658200597184678981709365472187109555648000000	1	1
131640119428935796341873094437421911128000000	1	1
263280238857871592683746188875843822256000000	1	1
526560477715743185367492377751686764512000000	1	1
105312095543148637073488675550337352824000000	1	1
210624191086297274146977351100674705648000000	1	1
421248382172594548293954702201349411296000000	1	1
842496764345189096587909404402698822592000000	1	1
1684993528690378193175818808805397645184000000	1	1
3369987057380756386351637617610795290368000000	1	1
6739974114761512772703275235221590580736000000	1	1
1347994822952302554540655047044381171472000000	1	1
2695989645904605109081310094088762342944000000	1	1
5391979291809210218162620188177524685888000000	1	1
10783958583618420436325203763550493377776000000	1	1
21567917167236840872650407527100986755552000000	1	1
43135834334473681745300815054201973511104000000	1	1
86271668668947363490601630108403947022208000000	1	1
172543337337894726953003260216807894044416000000	1	1
34508667467578945390600652043361578808832000000	1	1
6901733493515789078120130408672315761664000000	1	1
1380346698703157815624026081734463152328000000	1	1
2760693397406315631248052163468926304656000000	1	1
552138679481263126249610432693785260912000000	1	1
1104277358962526252496208665387570521824000000	1	1
2208554717925052504992417330775141043648000000	1	1
4417109435850105009984834661550282087376000000	1	1
8834218871700210019969669323100564174752000000	1	1
1766843774340042003993933864620112834944000000	1	1
3533687548680084007987867729240225668888000000	1	1
7067375097360168001975735458480445337776000000	1	1
1413475019472032003951467811696088665552000000	1	1
282695003894406400790293562339217733104000000	1	1
565390007788812800190587124678435466208000000	1	1
113078001557762560038017424935687093216000000	1	1
22615600311552512007603484987137418632000000	1	1
45231200623051024015206969974274837264000000	1	1</td

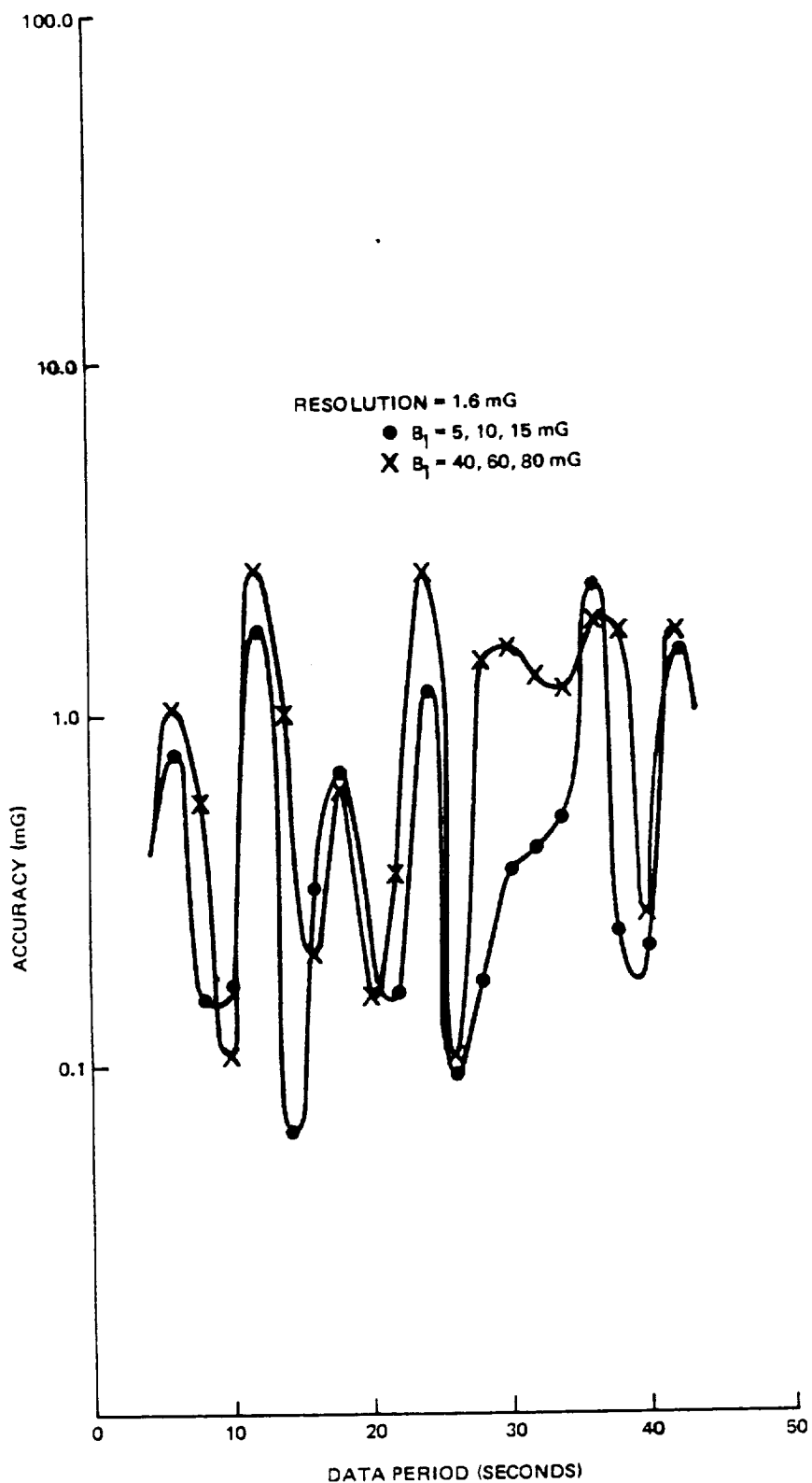
The column headed "Total Deviation" reports the root-mean-square (RMS) magnitude of the deviation in units of milligauss, and total deviation defined here is the same as "accuracy" as defined in Equation 6-1.

The test data spanned the perigee time and was taken from a constant 1000-second (16 minutes, 40 seconds) interval for all tests. Thus, as the simulated data period is increased, the total number of data points is decreased to maintain a constant total time interval of 1000 seconds.

Figures 6-1 through 6-5 show the simulated accuracy (mG) of the RESIDG algorithm for the granularity values of 1.6, 3.2, 5.0, 8.0, and 14.0 mG over the range of data periods simulated (6 to 42 seconds). Figures 6-1 and 6-5 are plots of the values in the Total Deviation column in Table 6-3.

These figures show the striking correlation between bias determination accuracy and data period. The accuracy is observed to be periodic with a period of 6 seconds (the spin period of the AMPTE spacecraft) for all resolutions. Also, the amplitude of oscillation generally is independent of the data period for a given resolution. The peaks of the oscillations occur at 6, 12, 18, 24, 30, 36, and 42 seconds. In a few cases, peaks appear as shoulders and are not completely distinct. When the data period is a multiple of 6 seconds, each magnetometer data sample is nearly the same as in previous samples; thus, this results in poor geometry for the least-squares algorithms. The best geometry occurs when successive readings differ by 180 degrees (e.g., a 9-second data period).

The results using the RESIDT algorithm qualitatively were the same as for the RESIDG algorithm. The behavior of the RESIDT algorithm showed the same oscillatory behavior as a function of data period.



8035/81

Figure 6-1. Simulated Accuracy of RESIDG for Granularity Value of 1.6 mG

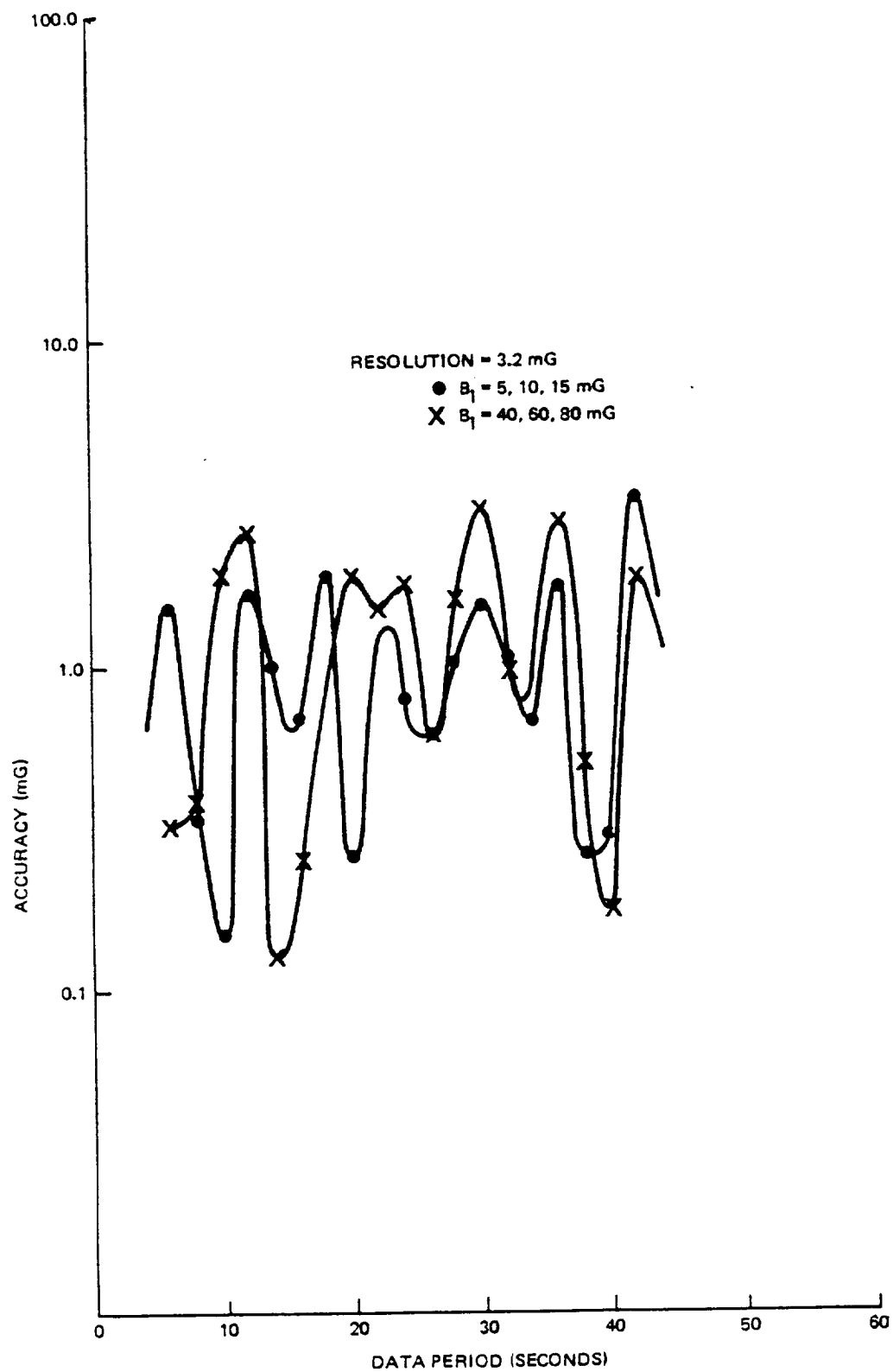


Figure 6-2. Simulated Accuracy of RESIDG for Granularity Value of 3.2 mG

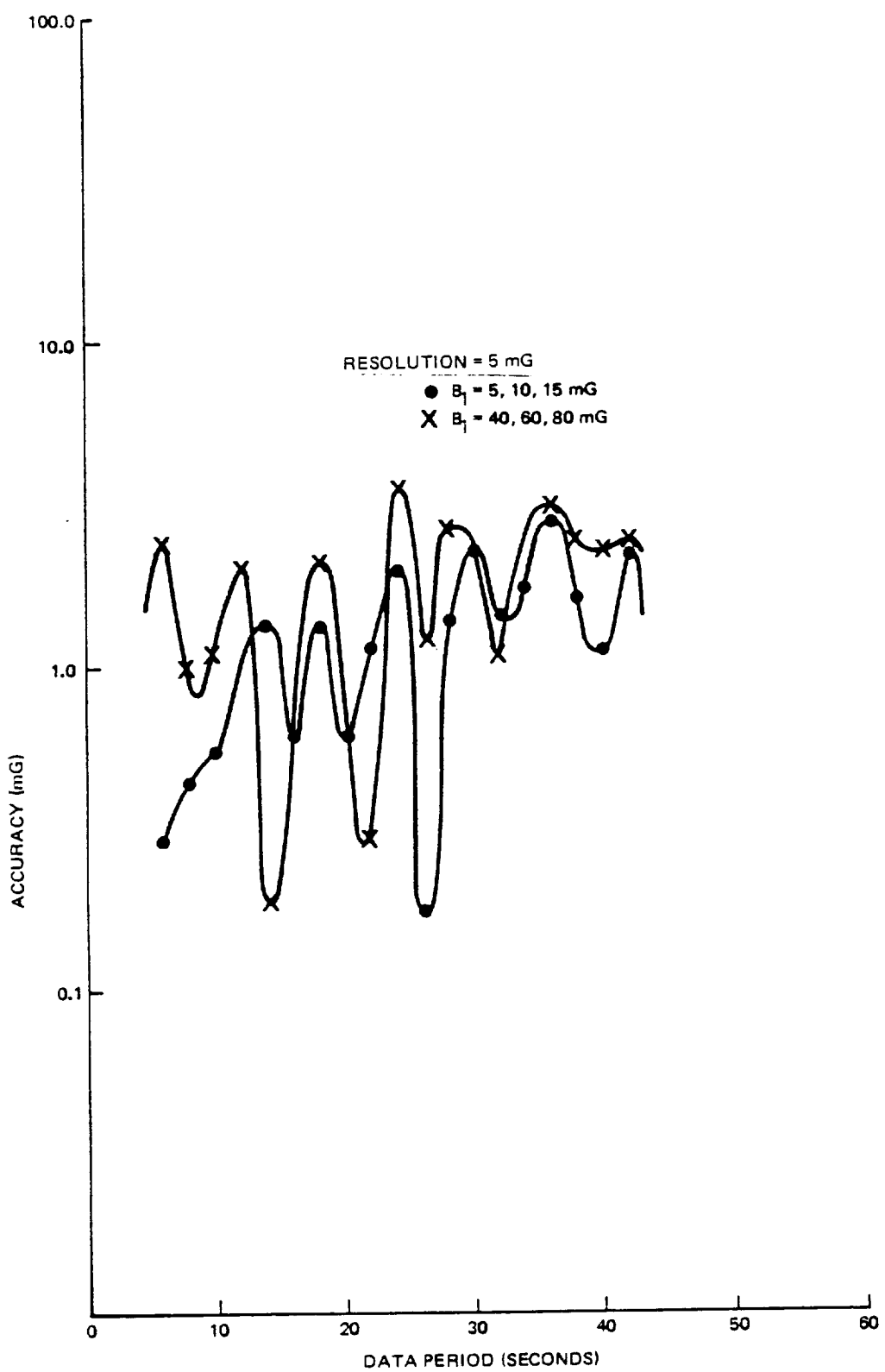


Figure 6-3. Simulated Accuracy of RESIDG for Granularity Value of 5.0 mG

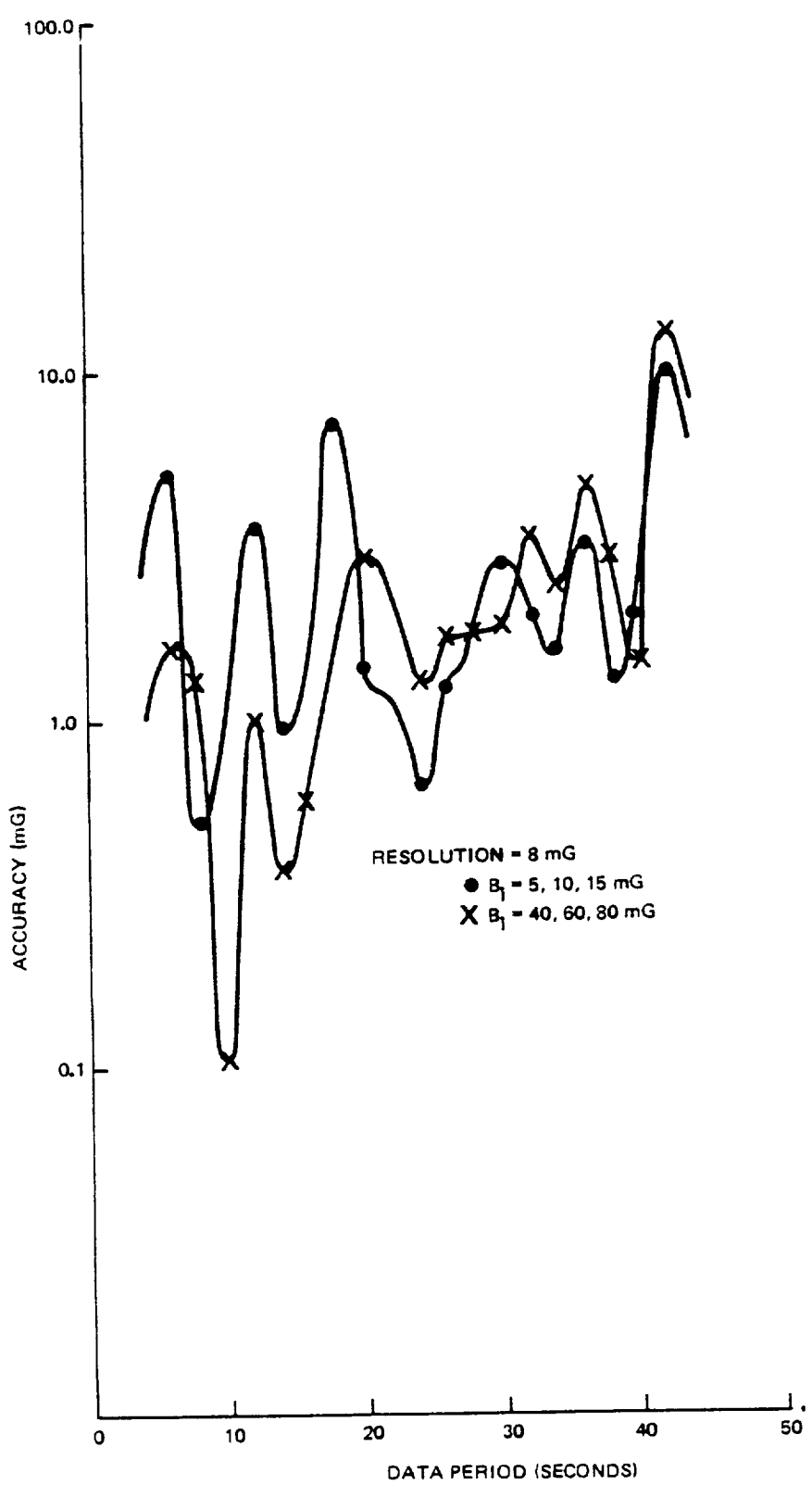


Figure 6-4. Simulated Accuracy of RESIDG for Granularity Value of 8.0 mG

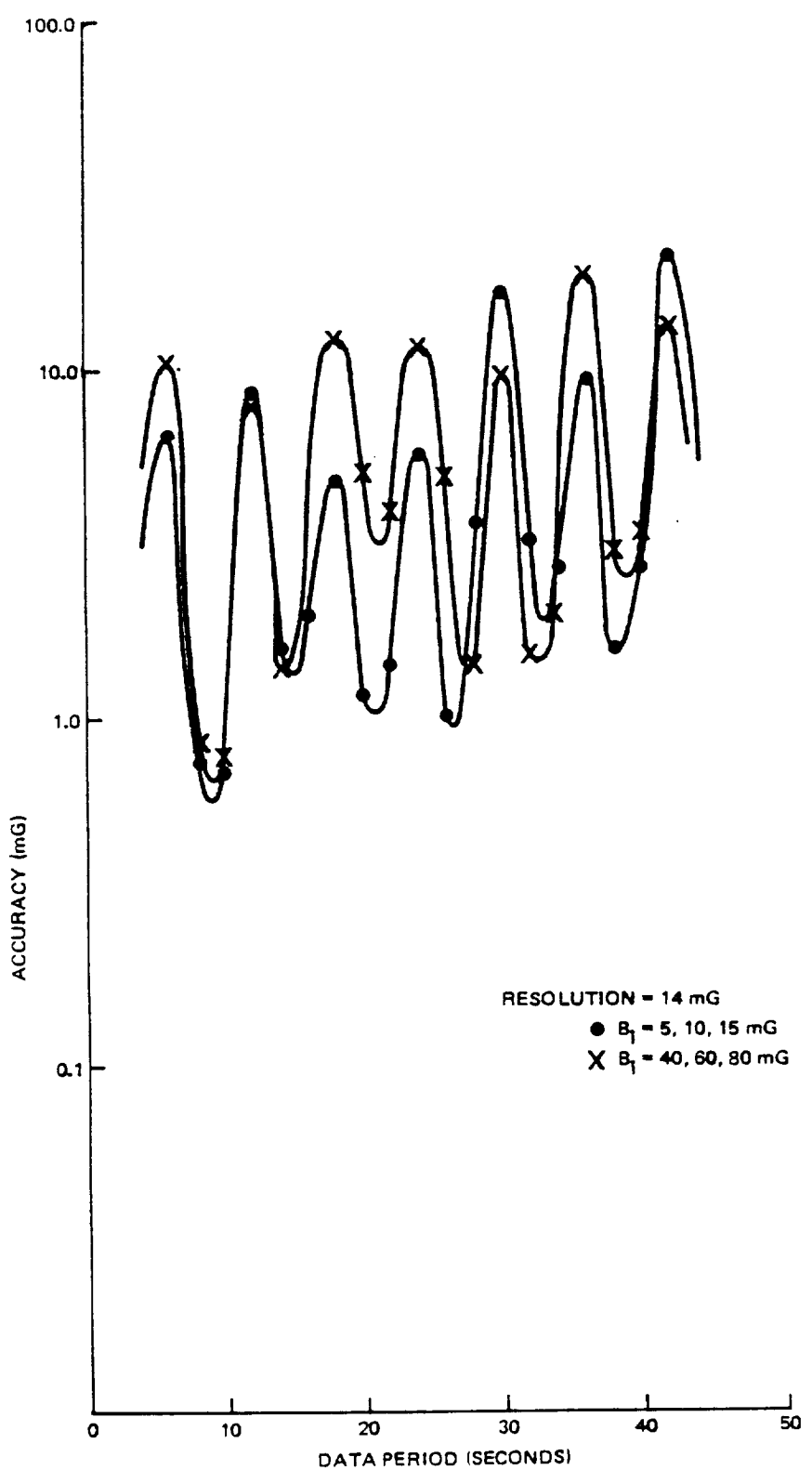


Figure 6-5. Simulated Accuracy of RESIDG for Granularity Value of 14.0 mG

Figures 6-6 and 6-7 show both the RESIDG and RESIDT results for 1.6 mG granularity and the 5, 10, 15 mG and 40, 60, 80 mG bias vectors. For the 5, 10, 15 mG case, both algorithms give almost identical results, with RESIDT giving better results near the peaks. For the 40, 60, 80 mG case, RESIDG gives far better results than RESIDT. This is because the RESIDG initial bias estimate is much more accurate than that used by RESIDT for large biases. However, both RESIDT and RESIDG give good results for the "good geometry" data periods (data periods that result in minimum values of the oscillation in accuracy), even when the relatively large bias vector of 40, 60, 80 mG is present.

With regard to accuracy versus sensor granularity alone, no universal curve appears to describe accuracy versus granularity for a specific data period (Figure 6-8). However, accuracy gets worse as the granularity increases, and granularities greater than 5 mG lead to large errors for the 6- and 12-second data periods. Figure 6-8 does enable one significant conclusion. The overall accuracy is much more dependent on a judicious choice of data period rather than on sensor granularity. Even for a "poor" sensor granularity value (e.g., 8 mG or 14 mG), the accuracy of the RESIDG algorithm is good for data periods that are not multiples of the spacecraft spin rate (e.g., 8-, 10-, or 14-second data periods illustrated in Figure 6-8).

6.5 NONPROXIMITY TO PERIGEE TEST RESULTS

Several tests were run to determine the effect of varying the data collection time period (1000-second duration) over different locations within the simulated highly elliptical AMPTE orbit. Specifically, the purpose of the test was to determine the effects of not spanning perigee time during the data collection period.

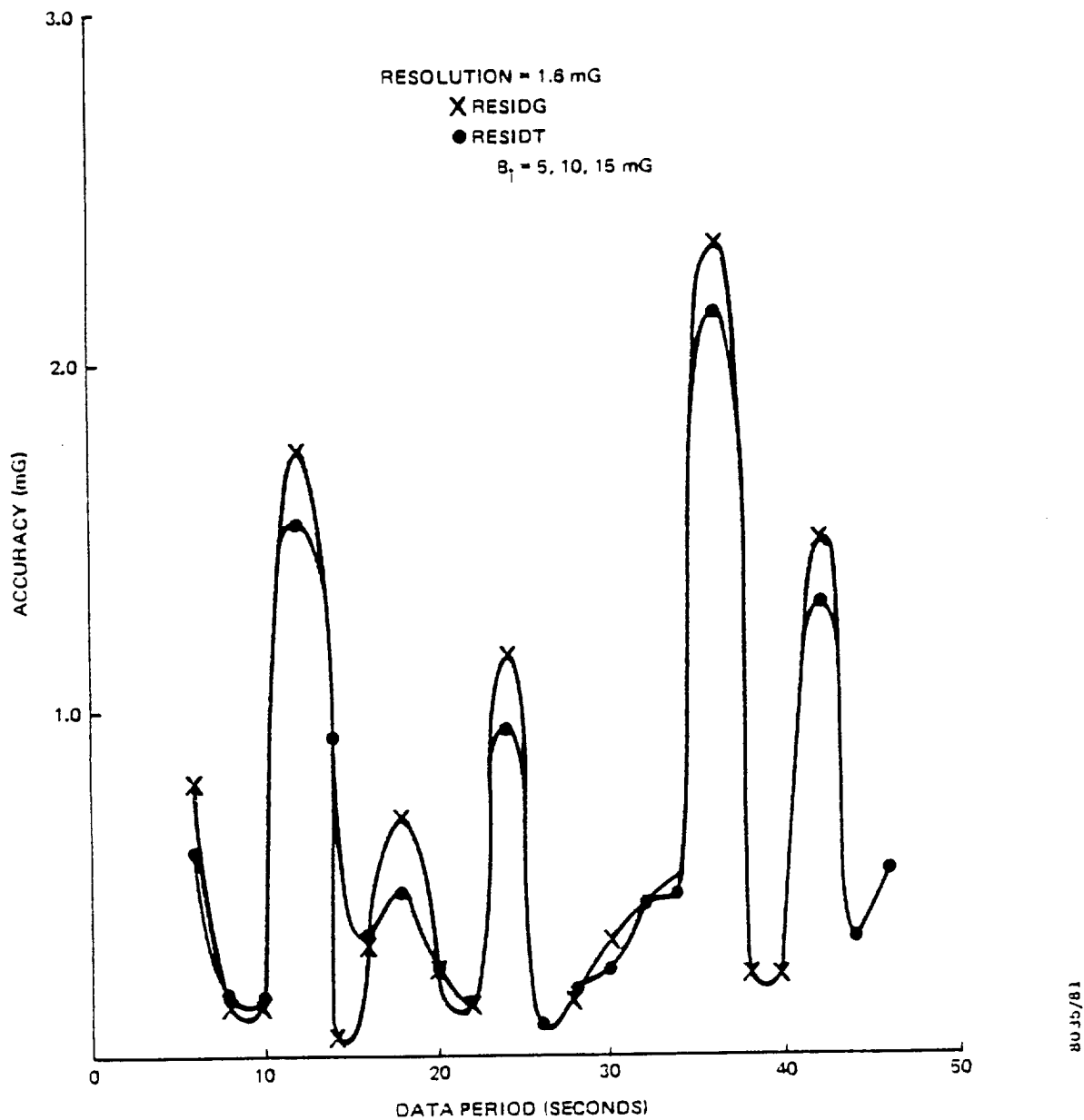


Figure 6-6. RESIDG and RESIDT Results for 1.6 mG Granularity (Bias Vector = 5, 10, 15 mG)

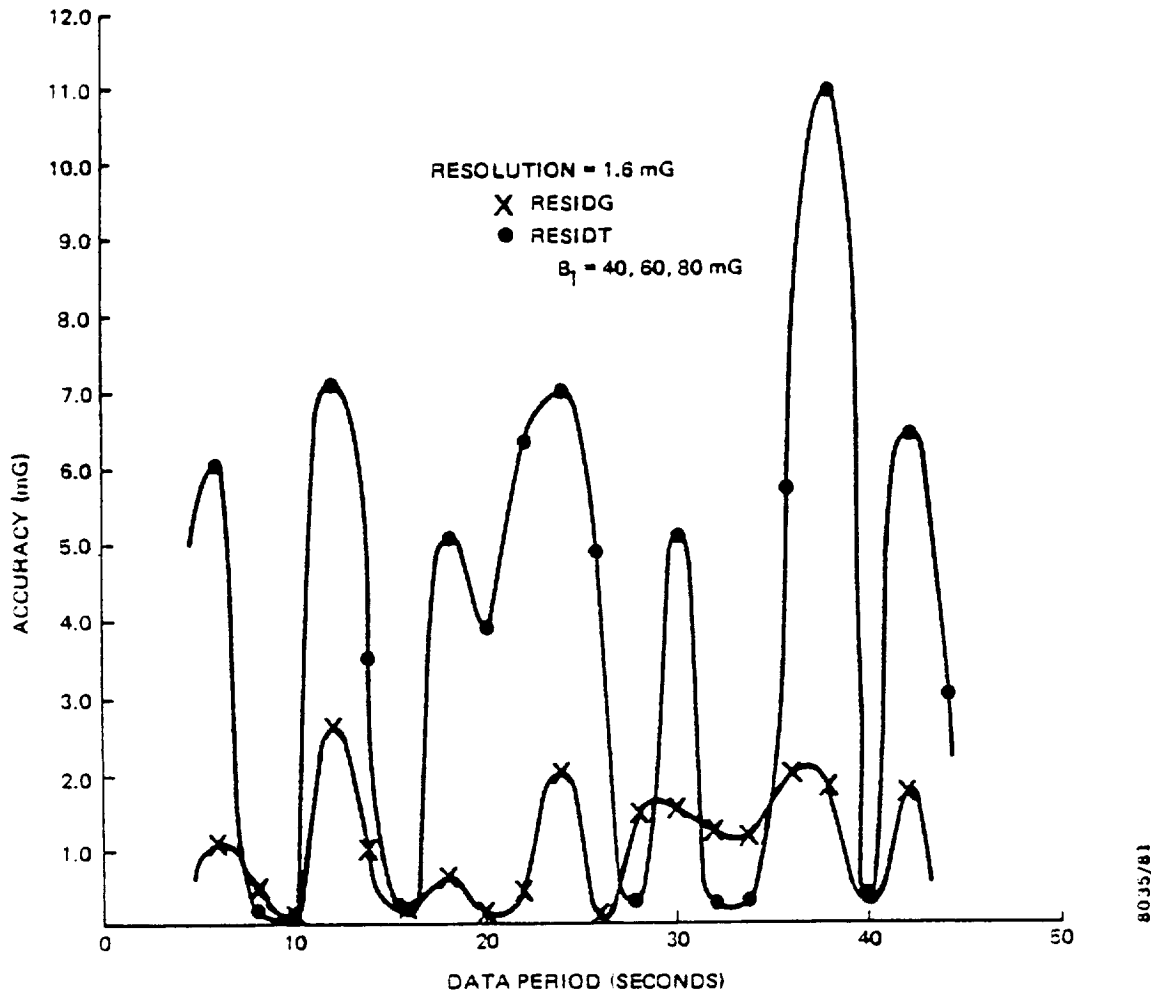


Figure 6-7. RESIDG and RESIDT Results for 1.6 mG
Granularity (Bias Vector = 40, 60, 80 mG)

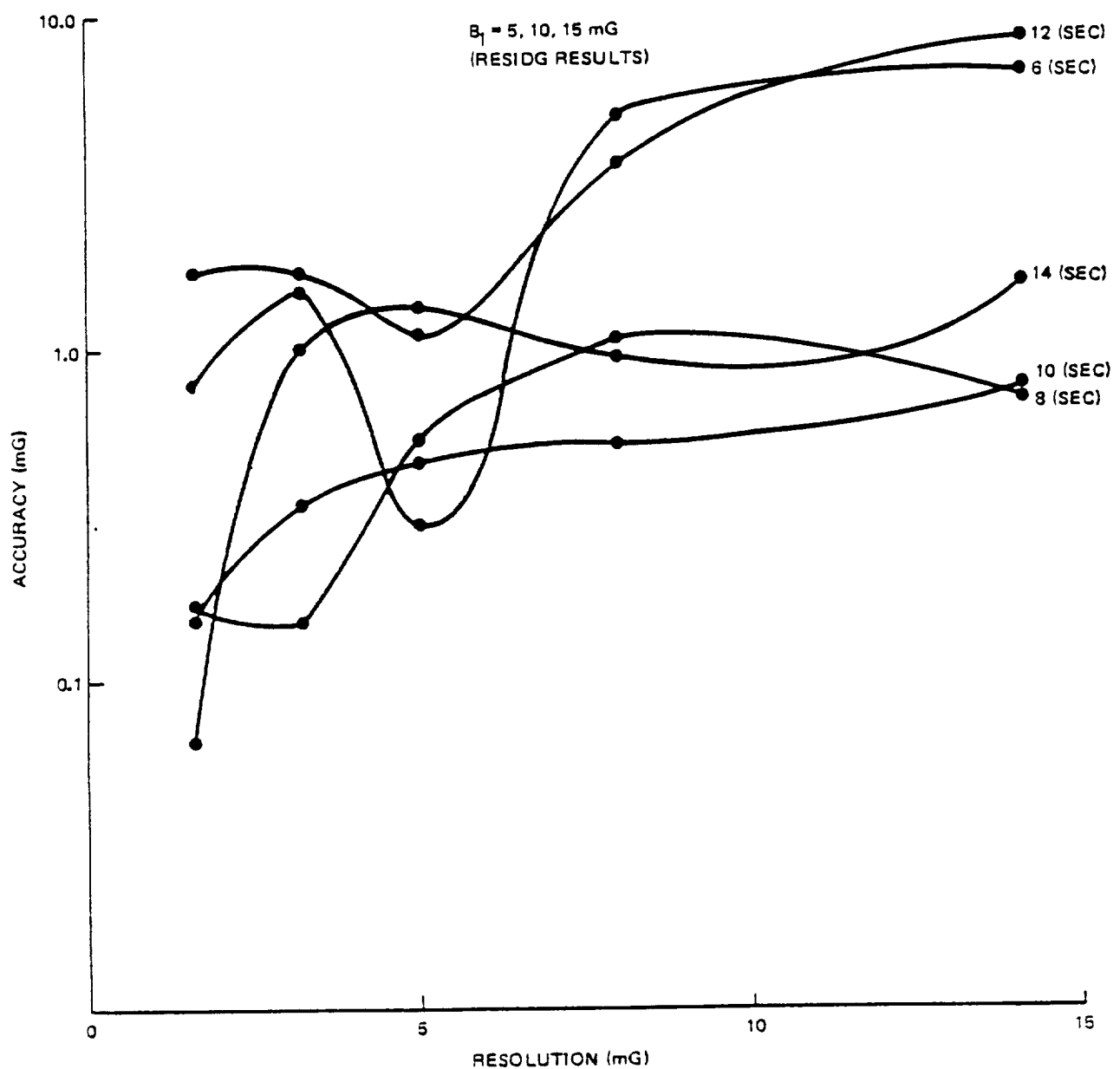


Figure 6-8. Accuracy Versus Sensor Granularity

All tests used a 1000-second data collection period (16 minutes, 40 seconds) beginning at times (YYMMDD.HHMM) ranging from 830901.0000 to 830901.0130 (Tables 6-5 and 6-6). The perigee time assumed was 830901.0138. For each simulation, at 15-minute intervals (830901.0000, 830901.0015, ... 830901.0130), a sensor granularity of 3.2 mG and a data period of 10 seconds were used. Tests were performed for x, y, z bias vectors of 5, 10, 15 and 40, 60, 80 mG. Note that the test with the starting time of 830901.0130 is the one that spans the perigee time. "Accuracy" in Tables 6-5 and 6-6 is the same as defined by Equation (6-1).

Figure 6-9 presents a plot of the computed accuracy versus start time. Figure 6-9 illustrates that accuracy is indeed dependent on proximity to perigee. Data taken at a starting time 40 minutes before perigee (or closer to perigee) was much more accurate than data taken 1 hour or more before perigee.

Two other observations are apparent from Figure 6-9. First, accuracy is dependent on bias magnitude. For the 10-second simulated data period the results for the 5, 10, 15 mG bias vector were in general half an order of magnitude (or more) better than the 40, 60, 80 mG case. Even for data taken 1 hour away from perigee, the accuracy for the 5, 10, 15 mG bias case was acceptable on the order of a few milligauss. The second additional observation is that the RESIDG and RESIDT algorithms performed roughly equivalently; neither algorithm was significantly superior to the other either close to or away from perigee.

6.6 SENSOR MISALIGNMENT TEST RESULTS

Several tests were made to determine the effects of magnetometer misalignment. The x-axis was misaligned in the x-y plane toward the y-axis; the y-axis was misaligned in the

Table 6-5. RESIDG Orbit Dependence Results

START TIME (HHMMSS)	SIMULATED BIASES (mG)			COMPUTED BIASES (mG)			DEVIATIONS (mG)			ACCURACY (mG)
	X	Y	Z	X	Y	Z	X	Y	Z	
.013000	5	10	15	5.00	10.01	14.81	.00	.01	-.19	.19
	40	60	80	39.95	59.17	79.84	-.05	-.83	-.16	.85
.011500	5	10	15	4.97	10.33	14.99	-.03	.33	-.01	.33
	40	60	80	40.13	59.34	79.86	.13	-.66	-.14	.69
.010000	5	10	15	4.86	9.59	15.05	-.14	-.41	.05	.44
	40	60	80	39.67	52.30	79.86	-.33	-.70	-.14	7.70
.004500	5	10	15	5.08	5.33	15.01	.08	-.67	.01	4.67
	40	60	80	37.65	46.78	75.27	-.35	-.35	-.22	4.73
.003000	5	10	15	4.98	7.24	14.95	.02	-.26	-.05	2.76
	40	60	80	35.69	48.74	71.42	-.40	-.17	-.58	14.80
.001500	5	10	15	4.96	7.83	14.92	-.04	-.17	-.08	2.17
	40	60	80	35.42	49.35	70.28	-.48	-.65	-.72	15.12
.000000	5	10	15	4.69	8.31	14.51	-.31	-.69	-.49	1.79
	40	60	80	34.84	49.67	69.60	-.16	-.33	-.40	15.54

GRANULARITY = 3.2 mG
 DATA PERIOD = 10.0 SECONDS
 PERIGEE TIME = .013800
 DATA COLLECTION PERIOD = 1000 SECONDS

18/9308

Table 6-6. RESIDT Orbit Dependence Results

START TIME (HHMMSS)	SIMULATED BIASES (mG)			COMPUTED BIASES (mG)			DEVIATIONS (mG)			ACCURACY (mG)
	X	Y	Z	X	Y	Z	X	Y	Z	
.013000	5	10	15	5.00	10.02	14.81	-.00	.02	-.19	.19
	40	60	80	39.96	58.91	79.86	-.04	-1.09	-.15	1.10
.011500	5	10	15	4.97	10.40	15.00	-.03	.40	.00	.40
	40	60	80	40.16	59.92	79.93	.16	-.08	-.07	.19
.010000	5	10	15	4.86	10.02	15.05	-.14	.02	.05	.15
	40	60	80	39.86	61.21	80.20	-.14	1.21	.20	1.23
.004500	5	10	15	5.08	6.73	15.00	.08	-3.27	.00	3.27
	40	60	80	40.20	46.38	80.10	.20	-13.63	.10	13.63
.003000	5	10	15	5.00	8.33	14.98	.00	-1.67	-.02	1.67
	40	60	80	40.00	46.48	79.97	.00	-13.52	-.03	13.52
.001500	5	10	15	4.99	7.76	15.03	-.01	-2.24	.03	2.24
	40	60	80	39.64	46.60	80.14	-.36	-13.40	.14	13.41
.000000	5	10	15	4.62	8.67	14.79	-.38	-1.33	-.21	1.40
	40	60	80	39.90	46.56	79.68	-.10	-13.44	-.32	13.45

GRANULARITY

= 3.2 mG

DATA PERIOD

= 10.0 SECONDS

PERIGEE TIME

= .013800

DATA COLLECTION
PERIOD

= 1000 SECONDS

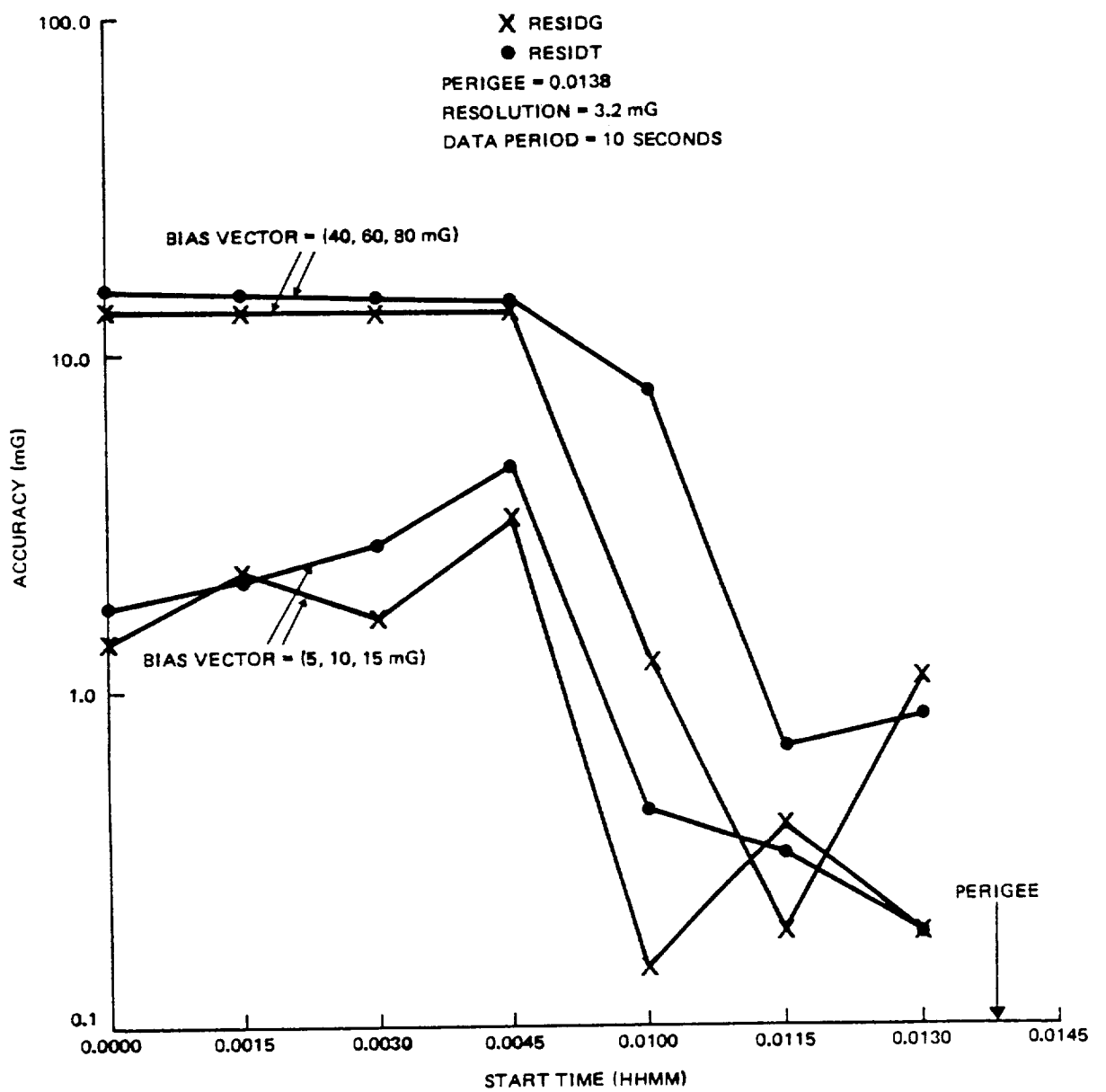


Figure 6-9. Computed Accuracy Versus Start Time for RESIDG and RESIDT

x-y plane toward the x-axis; the y-axis was misaligned in the y-z plane toward the z-axis; and, the y-axis was misaligned out of the x-y and y-z planes. Table 6-7 shows the results of these tests. The tests were run with an x, y, z component bias of 5, 10, and 15 mG; 3.2 mG sensor granularity; and a data period of 10 seconds.

The tests in Table 6-7 show that as the x-axis is rotated toward the y-axis in the x-y plane, the error seen is almost linear as a function of the angle (Figure 6-10). In this situation, the x and y biases are coupled together, while the z bias is almost unaffected by the misalignment. This occurs because the bias determination algorithms are attempting to adjust the biases such that the magnitude of the measured field in the x-y plane is the same as the computed field. Because the z-bias has no effect on the component of the field in the x-y plane, it is not adjusted erroneously in an attempt to compensate for the misalignment; the x and y biases are adjusted erroneously.

The same effect was noticed when the y-axis was rotated in the x-y plane toward the x-axis. When the y-axis was rotated toward the z-axis in the y-z plane, the y and z biases were adjusted by the algorithms to compensate for misalignment (Table 6-7). When a general rotation of the y-axis was performed such that the y-axis lies out of both the x-y and y-z planes, all biases were adjusted.

Table 6-7. Effects of Magnetometer Misalignment

MISALIGNMENT (DEGREES)	COMPUTED BIASES (mG)			DEVIATIONS (mG)			ACCURACY (mG)	ALGORITHM
	X	Y	Z	X	Y	Z		
X-AXIS (TOWARD Y-AXIS IN X-Y PLANE)								
1	3.80	10.32	14.91	-1.20	.32	-.10	1.24	RESIDG
2	3.80	10.36	14.90	-1.20	.36	-.10	1.25	RESIDT
2	2.60	10.48	15.00	-2.40	.47	.00	2.45	RESIDG
2	2.60	10.45	14.99	-2.40	.45	.01	2.45	RESIDT
3	1.58	10.69	14.98	-3.43	.69	-.02	3.49	RESIDG
3	1.57	10.67	14.98	-3.43	.67	-.02	3.49	RESIDT
4	.12	11.11	15.05	-4.88	1.11	.06	5.01	RESIDG
4	.12	11.08	15.05	-4.88	1.08	.06	5.00	RESIDT
5	-.80	11.32	15.19	-5.80	1.32	.19	5.95	RESIDG
5	-.80	11.30	15.19	-5.80	1.30	.19	5.95	RESIDT
Y-AXIS (TOWARD X-AXIS IN X-Y PLANE)								
1	4.00	10.14	14.79	-1.00	.14	-.21	1.03	RESIDG
1	4.00	10.15	14.79	-1.00	.15	-.21	1.04	RESIDT
2	2.72	10.18	14.75	-2.29	.18	-.25	2.31	RESIDG
2	2.71	10.20	14.75	-2.29	.20	-.25	2.31	RESIDT
3	1.51	9.76	14.62	-3.49	-.24	-.38	3.52	RESIDG
3	1.51	9.79	14.62	-3.49	-.21	-.38	3.52	RESIDT
4	.40	9.65	14.49	-4.60	-.35	-.51	4.64	RESIDG
4	.40	9.66	14.49	-4.60	-.34	-.51	4.64	RESIDT
5	-.71	9.35	14.44	-5.71	-.65	-.56	5.78	RESIDG
5	-.72	9.36	14.44	-5.72	-.64	-.56	5.78	RESIDT
Y-AXIS (TOWARD Z-AXIS IN Y-Z PLANE)								
5	5.03	9.27	9.28	.03	-.73	-.572	5.78	RESIDG
5	5.03	9.28	9.28	.03	-.72	-.572	5.77	RESIDT
Y-AXIS (GENERAL ROTATION)								
$\alpha = 87^\circ$	1.24	9.37	10.15	-3.76	-.63	-4.85	6.16	RESIDG
$\beta = 5^\circ$	1.24	9.39	10.15	-3.76	-.61	-4.85	6.16	RESIDT
$\delta = 86^\circ$								

18/9808

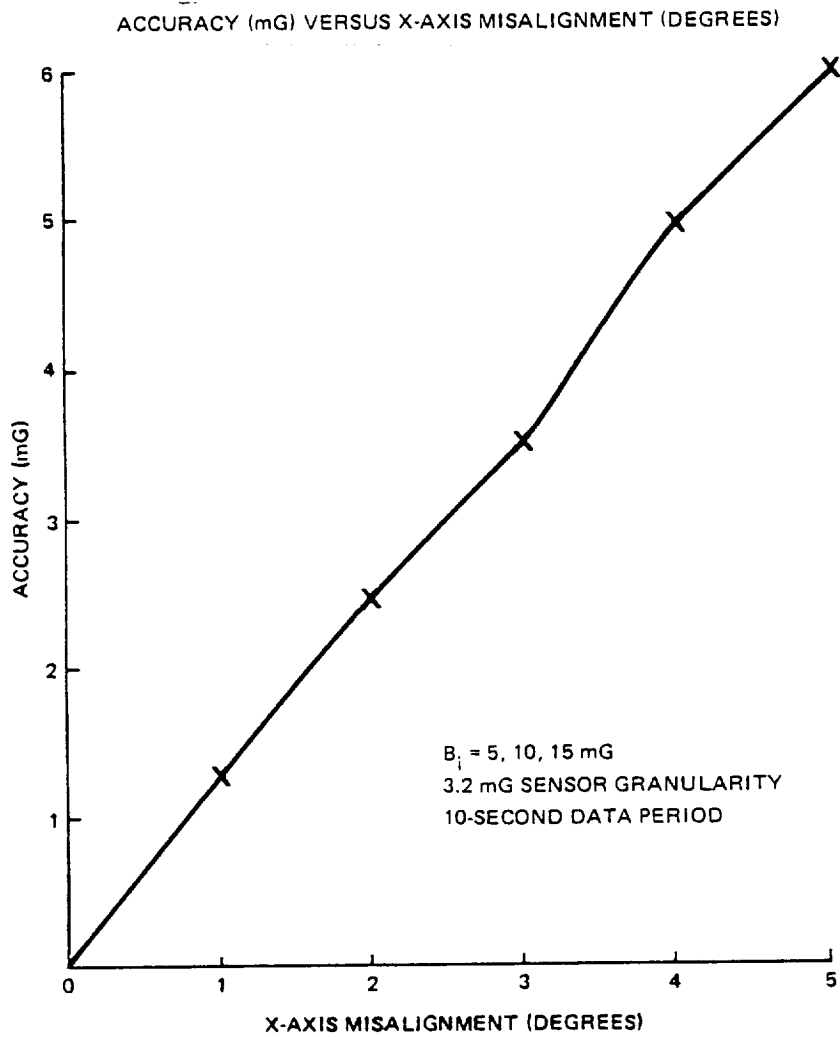


Figure 6-10. Computed Accuracy Versus X-Axis Misalignment

SECTION 7 - CONCLUSIONS

On the basis of this study, several conclusions are presented.

7.1 SENSITIVITY TO DATA PERIOD

Selection of a "good" data period for the CCE magnetometer data readings is the single most critical factor in obtaining accurate magnetometer bias determination results. The accuracy of the results is more sensitive to data period than any other effect (i.e., sensor granularity, magnetometer bias, or sensor misalignment).

In the tests for sensitivity to data period (using data periods ranging from 6 to 42 seconds in increments of 2 seconds), the accuracy oscillated over an order of magnitude. The worst-case data period is equal to the spin period of the spacecraft plus multiples of the spin period (in this case, $6\text{ seconds} + n \cdot 6\text{ seconds}$, $n = 0, 1, 2\dots$). The best-case data period would be such that successive magnetometer readings are taken when the spacecraft has rotated π radians (180°) relative to the previous reading (e.g., a 9-second data period plus multiples of 6 seconds). (See Figures 6-1 through 6-5).

7.2 SENSITIVITY TO SENSOR GRANULARITY

Bias determination accuracy does depend somewhat on sensor granularity, but not as much as on data period. Figures 6-1 through 6-5 illustrate that the general trend is toward less accuracy as the granularity increases; however, for good data periods (minimums of the oscillations), the values of the accuracy were excellent (about 1 mG or less) even for granularities as high as 14 mG.

A granularity of 5.0 mG or less is recommended for the AMPTE mission. Good results were obtained for granularity values

of 1.6 mG, 3.2 mG, and 5.0 mG, even when a poor data period (6 or 12 seconds) was used (Figure 6-8). Large errors may occur if the sensor granularity is large, particularly if a poor data period is chosen.

7.3 SENSITIVITY TO MAGNETOMETER BIASES

High magnetometer biases (e.g., up to a 40, 60, 80 mG, x, y, z bias vector), in general, do not seem to be a significant problem for the RESIDG and RESIDT algorithms used in this study, particularly when the data spans perigee. For the sensor granularities of 1.6 mG through 14.0 mG, the results (Figures 6-1 through 6-5) indicate that higher bias magnitude (e.g., a 40, 60, 80 mG bias vector) results in only slightly worse accuracy than a lower bias magnitude (e.g., a 5, 10, 15 mG bias vector). For the above cases, data period is a far more important effect than magnetometer bias. For data taken substantially away from perigee (e.g., 1 hour or more), high magnetometer bias does result in poor accuracy; however, utilization of data that far away from perigee is not recommended.

7.4 SENSITIVITY TO PERIGEE PROXIMITY

For the AMPTE mission, it is recommended that the major data collection period be confined to a window of about ± 25 minutes from perigee, the region in which the principal component of the geomagnetic field is about 50 mG or greater (Figure 5-2). Figure 6-9 illustrates that good results may be obtained as much as 40 minutes away from perigee, if the bias magnitude is not high. However, good results (an accuracy of about 1 mG) were obtained for both the high and low magnetometer bias cases for the data taken within 25 minutes of perigee.

7.5 SENSITIVITY TO SENSOR MISALIGNMENT

The effects of misalignment of the x- and y-axis magnetometers are significant. In the range simulated (0 to 5 degrees), an error of about 1 mG resulted per each degree of misalignment.

7.6 RECOMMENDED BIAS DETERMINATION ALGORITHM

For small magnetometer biases (e.g., a 5, 10, 15 mG bias vector), the RESIDG and RESIDT algorithms performed roughly the same qualitatively. Both algorithms show the oscillatory behavior described above as a function of data period. For larger magnetometer biases (e.g., a 40, 60, 80 mG bias vector), RESIDG gives significantly better performance than does RESIDT (Figures 6-7 and 6-9). However, for good data periods, both RESIDG and RESIDT perform well even when large biases are present.

The recommended bias determination algorithm is to use the RESIDT iteration method with the option to use the RESIDG trial solution. For large biases the RESIDG initial bias estimate is more accurate than that used by RESIDT. However, RESIDT was found to be more stable than RESIDG. There were no cases found in this study in which RESIDT diverged. RESIDG did diverge in several cases where large magnetometer biases were present.

7.7 NECESSITY FOR SIMULTANEOUS DATA READINGS

Because the CCE spacecraft is rotating, it is necessary that the three readings from the magnetometer triad be obtained simultaneously for use with the magnetometer bias determination algorithms tested in this study. This requires either that the three readings occur simultaneously in the telemetry data, or that each of the readings be accurately time-tagged such that all three readings can be rotated to a common time using the known spin rate.

REFERENCES

1. Computer Sciences Corporation, CSC/TM-80/6159, Solar Maximum Mission (SMM) Attitude Analysis Postlaunch Report, G. Nair, R. Thompson, P. Gambardella, G. Neal, Y. Kwon, P. Kammeyer, and J. Buckley, August 1980
2. --, CSC/TM-81/6069, Active Magnetospheric Particle Tracer Explorers (AMPTE) Engineering Data Simulator Description and User's Guide, G. Neal and R. Thompson, April 1981
3. National Aeronautics and Space Administration, GSFC, Executive Phase Project Plan for Active Magnetospheric Particle Tracer Explorers, G. Ousley, August 1980
4. Computer Sciences Corporation, 3000-32700-01TM, Determination of Magnetometer Biases Using Module RESIDG, G. Gambhir, March 1975
5. Goddard Space Flight Center, Volume I Mission and Data Operations IBM 360 User's Guide, J. Balakirsky, December, 1978